Research article

Asymptotic analysis of compression sensing in ionic polymer metal composites: The role of interphase regions with variable properties

Valentina Volpini and Lorenzo Bardella[*]

Department of Civil, Environmental, Architectural Engineering and Mathematics, University of Brescia, via Branze, 43, 25123 Brescia, Italy

* **Correspondence:** Email: lorenzo.bardella@ing.unibs.it; Tel: +390303711238.

Abstract: Ionic Polymer Metal Composites (IPMCs) consist of two noble metal electrodes plating an electroactive polymeric membrane, referred to as ionomer, which is electroneutralised by a solvent including mobile ions. The IPMC manufacturing leads to thin interphase regions next to the electrodes, the so-called Composite Layers (CLs), in which metal atoms occupy interstitial sites within the ionomer. In this work we extend previous efforts of our group on IPMC compression sensing to include the important effect of CLs, where large variations of the electrochemical properties occur. In IPMC compression sensing the application of a through-the-thickness displacement leads to a short-circuit electric response, here assumed to be governed by a linearised *modified* Poisson-Nernst-Planck (PNP) system of partial differential equations (PDEs), to be solved for the time-evolving electric potential and mobile ions concentration as functions of the displacement field evaluated through the linear momentum balance. The variation of material properties in the CLs requires the simultaneous integration of the governing system of PDEs in three regions: the membrane and the two CLs. To this purpose, we resort to the perturbative method of matched asymptotic expansions. Except for a numerical inverse Laplace transform, this allows us to obtain an analytical solution through which we establish an equivalent circuit model elucidating the main features of the IPMC sensing behaviour. We validate and discuss the analytical solution through comparison with finite element analyses, whereby we also numerically solve the nonlinear modified PNP systems fully coupled with the linear momentum balance accounting for the electrochemical stresses. We finally provide some insight into the role of CLs in the IPMC sensing behaviour, by assessing its sensitivity to some key parameters. We expect the obtained results to aid the design of optimised IPMC sensors.

Keywords: ionic polymer metal composite; composite layer; sensing; electrochemomechanics; Poisson-Nernst-Planck system; boundary layer; perturbative problem; matched asymptotic expansion; finite element method

1. Introduction

Ionic Polymer Metal Composites (IPMCs) are transducers whose electroactive behaviour is guaranteed by an electrically charged ionomeric membrane infused with a solvent containing mobile ions. These ions are referred to as counterions because they electroneutralise the membrane, which is sandwiched between electroplated noble metal electrodes [1, 2]. In most cases, the employed materials are Nafion or Flemion for the membrane (a few hundreds of micrometres thick and containing negative fixed ions), water for the solvent, lithium or sodium for the (positively charged) counterions, and gold or platinum for the electrodes [3].

To describe the IPMC behaviour, in this investigation we adopt the Cha and Porfiri [4] electrochemomechanical theory. In this theory, the counterions motion governs both sensing and actuation through ions accumulation or depletion in the proximity of the ionomer-electrode interfaces, forming the so-called *boundary layers*. These layers occupy membrane regions whose thickness is on the order of the Debye screening length and are associated with the double-layer charging occurring therein [5, 6]. In sensing, an applied mechanical deformation induces a counterions redistribution and a consequent charge storage at the ionomer-electrode interfaces, in turn generating a voltage drop across the electrodes. By short-circuiting the electrodes, this leads to a measurable electric current [7–10]. Dually, in actuation, an applied voltage drop across the electrodes leads to a counterions redistribution generating macroscopic deformation [11–14].

One of the most employed IPMC manufacturing processes is the electroless chemical reduction [3], whereby a metal salt diffuses in the ionomer, until final deposition at the external surface through a reducing agent. In the proximity of the ionomer-electrode interfaces, the presence of metal particles among the ionomer macromolecules modifies not only the stiffness of the membrane, but primarily its electrochemical properties, leading to an increased electric permittivity along with a decreased counterions diffusivity. In literature, these interphase regions are referred to as either intermediate layers [15] or Composite Layers (CLs) [16, 17]. Here, they are reported in the schematic of Figure 1, where, for the sake of clarity, they are overmagnified. CLs are indeed very thin layers, such that their thickness d (here assumed to be the same for both CLs) is much smaller than the thickness of the plain ionomer, $2h$, henceforth also referred to as the bulk of the membrane. By appropriately tuning the CL properties, CLs may be employed in the modelling even to account for the roughness of the ionomer-electrode interfaces, whose effect can also be partly described in Cha and Porfiri [4] theory by a steric coefficient governing the capability of counterions to accumulate at the interfaces [18–22].

In this work we extend the model developed in our contribution [23] which focuses on *compression sensing* under the assumption of spatially uniform electrochemical properties in the entire membrane. Compression sensing consists of the short-circuit electric signal in IPMCs subjected to a through-the-thickness compressive displacement. This test can be employed for the IPMC characterisation, such that the input can be for instance a sinusoidal function of time [23, 24]. By following the studies in [4] and [25] on IPMCs under bending, as a main novelty, here we investigate the role of CLs on IPMC compression sensing.
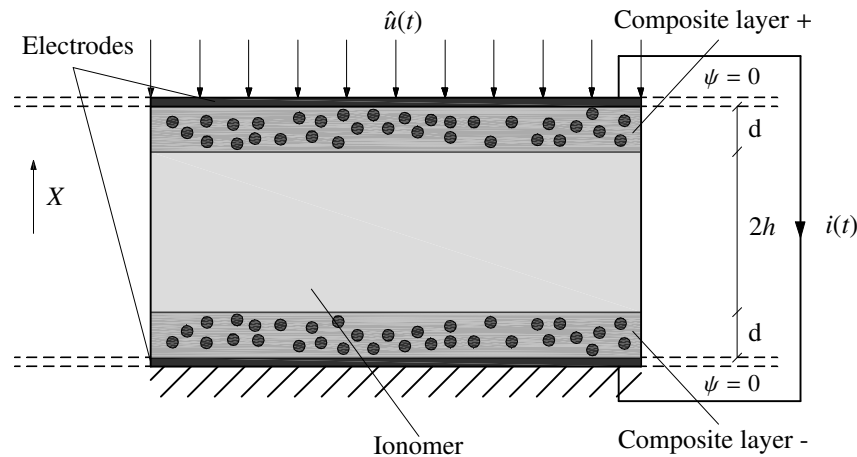
Figure 1. Schematic of IPMC compression sensing: geometric parameters and boundary/short-circuit conditions with reference to the undeformed state. The bottom face has fixed vertical displacement, whereas the top face is subjected to a known vertical displacement $\hat{u}(t)$. The ion-blocking condition holds at the CL-electrode interfaces. The electric current $i(t)$ is generated by short-circuiting the electrodes.

To this aim, we formulate three *modified* Poisson-Nernst-Planck (PNP) systems of partial differential equations (PDEs), governing the electrochemistry in the membrane bulk and in each CL (Section 2). Here, the term *modified* refers to the coupling between the displacement field and the electrochemical fields classically entering the conventional PNP system, i.e., the electric potential ψ and the counterions concentration C. In fact, the adopted Cha and Porfiri [4] theory relies on the definition of electrochemical stresses, related to ψ and C, that must be equilibrated by the mechanical stress, the latter being conjugate to the ionomer deformation. Hence, although the electrochemomechanical problem at hand should in general be solved by coupling the modified PNP system with the linear momentum balance, on the basis of our previous analysis [23] and IPMC sensing behaviour in general (see Porfiri [10] and references therein), we may obtain accurate results by first solving the linear momentum balance in terms of mechanical stress only and, then, by using the displacement field as an input for the modified PNP system. Moreover, we linearise the modified PNP systems, given that in IPMC sensing this is allowed for appropriately small applied displacement [10, 17, 23]. Then, a crucial step towards an asymptotic approach to solve the compression sensing problem consists of a meaningful nondimensionalisation of the governing equations (Section 2.2) aiming at singling out the difference in scale of membrane bulk, CLs, and boundary layers through suitably small parameters modulating the PDEs to solve.

Hence, in order to analytically solve the modified PNP systems, we resort to the method of matched asymptotic expansions [26], which is a powerful mathematical tool leading to accurate results when the PDEs to solve constitute a perturbative problem. We provide all the details concerned with the analytical solution in Section 3. Note that such solution, not fully explicit, requires the numerical computation of an inverse Laplace transform. In Section 3.4, we finally recast the obtained closed-form solution into an equivalent circuit model, which, by the way, allows us to highlight an essential feature of the displacement field needed to trigger a non-vanishing sensing response. Specifically, according

to the analogous result of [23], a short-circuit current is observed only if the membrane mechanical properties are such that the deformation field turns out to be different at the two ionomer-CL interface regions.

In Section 4, we validate the analytical solution. The validation is twofold. First, we particularise the new solution to the solution obtained in [23] for uniform electrochemical properties in the entire membrane. This requires the choice of appropriately small and large values of diffusivity and permittivity in the CLs. Second, we compare the results with those numerically obtained from a Finite Element (FE) analysis implementing the linearised modified PNP systems analytically solved.

The discussion in Section 5 assesses the limits of validity of the analytical solution by comparison with FE analyses of the fully coupled nonlinear PDEs constituted by the modified PNP system and the linear momentum balance (the latter involving the electrochemical stresses as well).

Finally, in Section 6, we investigate the role of some key parameters characterising the CLs. Specifically, by taking advantage of the analytical solution, we illustrate the results of some parametric analyses to provide insight on the efficiency of the present solution towards IPMC design and characterisation through inverse analysis. This is further elaborated in the concluding remarks offered in Section 7.

2. Governing equations

Under the hypotheses and boundary conditions assumed in [23], here summarised in Figure 1, the IPMC compression sensing is spatially one dimensional, such that the relevant fields vary along the through-the-thickness coordinate X, whose origin is placed in the ionomer midplane.

In the region $X \in [-h, h]$ identifying the membrane bulk, the following linearised modified PNP system holds [23]:

$$-\epsilon \, \frac{\partial^2 \psi(X,t)}{\partial X^2} = \mathcal{F}[C(X,t) - C_0] \tag{2.1a}$$

$$\mathcal{D}\left(\frac{\partial^2 C(X,t)}{\partial X^2} + \frac{\mathcal{F}C_0}{\mathcal{R}\mathcal{T}}\frac{\partial^2 \psi(X,t)}{\partial X^2} + \frac{C_0}{\nu - 1}\frac{\partial^3 u(X,t)}{\partial X^3}\right) = \frac{\partial C(X,t)}{\partial t} \tag{2.1b}$$

which has to be solved, as a function of time t, for the electric potential $\psi(X,t)$ and the counterions concentration $C(X,t)$, given the displacement field $u(X,t)$ obtained from the linear momentum balance. In Eqs (2.1), ϵ and $\mathcal{D}$ represent the electric permittivity and diffusivity, respectively, ν is the steric coefficient, C_0 is the uniform concentration of fixed ions, $\mathcal{F} = 96485$ C/mol is the Faraday constant, $\mathcal{R} = 8.314$ J/(mol K) is the gas constant, and $\mathcal{T}$ is the absolute temperature (always assumed to be equal to 300 K in this investigation). The steric coefficient $\nu \in [0, 1)$ macroscopically accounts for the capability of counterions to pack and accumulate against interfaces [18–22], with pile-up possibly influenced by roughness; $\nu = 0$ neglects steric effects and allows for unbounded ions accumulation at interfaces.

Equation (2.1a) is the Poisson equation, obtained by substituting in the Gauss law the electric displacement $D(X,t)$ written, through its constitutive law, in terms of electric potential. More specifically, the left-hand side of Eq (2.1a) is the divergence of $D(X,t)$, whose expression, linearised with respect to the geometry [23], reads

$$D(X,t) = -\epsilon \, \frac{\partial \psi(X,t)}{\partial X} \tag{2.2}$$

Equation (2.1b) is the Nernst-Planck equation, obtained by substituting in the mass balance the constitutive prescription for the counterions flux $J(X, t)$ in terms of counterions concentration and electric potential. More specifically, the left-hand side of Eq (2.1b) is the opposite of the divergence of $J(X, t)$, whose expression reads

$$J(X, t) = -\mathcal{D}\left(\frac{\partial C(X, t)}{\partial X} + \frac{\mathcal{F} C_0}{\mathcal{R} \mathcal{T}} \frac{\partial \psi(X, t)}{\partial X} + \frac{C_0}{\nu - 1} \frac{\partial^2 u(X, t)}{\partial X^2}\right) \tag{2.3}$$

Equation (2.3) is linearised with respect to both the geometry and the assumed small variation of $C(X, t)$ compared to C_0 [23]. This second linearisation leads to the second contribution at the right-hand side of Eq (2.3), accounting for the electrophoretic effect, whose nonlinearity may not in general be neglected in IPMC actuation [13, 14, 17, 25]. The last contribution in the flux (2.3) is due to the coupling between electrochemistry and mechanics [4, 23], in turn leading to the term involving the third derivative of the displacement field in the Nernst-Planck equation (2.1b). The nonlinear PDEs governing the fully coupled electrochemomechanical problem are provided in Section 5 where we numerically solve them to validate the analytical solution which constitutes the bulk of the present investigation.

Electric displacement and ion flux are strictly related to the short-circuit electric current generated in IPMC sensing. By referring to the generalised Ampère circuital law (see, e.g., [27]), in fact, the current in the ionomer, $i(t)$, is the sum of the so-called displacement current, due to the time-variation of $D(X, t)$, and a conduction current, related to $J(X, t)$, according to

$$i(t) = \frac{\partial D(X, t)}{\partial t} + \mathcal{F} J(X, t) \tag{2.4}$$

By following [16, 17], in the regions $X \in (h, h + d]$ and $X \in [-h - d, -h)$ identifying the CLs (see Figure 1) the modified PNP system and $i(t)$ turn out to be governed by the following relations, totally analogous to Eqs (2.1) and (2.4):

$$-\epsilon_{\pm}^{\text{cl}} \frac{\partial^2 \psi_{\pm}^{\text{cl}}(X, t)}{\partial X^2} = \mathcal{F}[C_{\pm}^{\text{cl}}(X, t) - C_0 \phi_{\pm}] \tag{2.5a}$$

$$\mathcal{D}_{\pm}^{\text{cl}}\left(\frac{\partial^2 C_{\pm}^{\text{cl}}(X, t)}{\partial X^2} + \frac{\mathcal{F} C_0 \phi_{\pm}}{\mathcal{R} \mathcal{T}} \frac{\partial^2 \psi_{\pm}^{\text{cl}}(X, t)}{\partial X^2} + \frac{C_0 \phi_{\pm}}{\nu - 1} \frac{\partial^3 u(X, t)}{\partial X^3}\right) = \frac{\partial C_{\pm}^{\text{cl}}(X, t)}{\partial t} \tag{2.5b}$$

$$i(t) = \frac{\partial D_{\pm}^{\text{cl}}(X, t)}{\partial t} + \mathcal{F} J_{\pm}^{\text{cl}}(X, t) \tag{2.6}$$

where the subscript $\pm$ identifies two unknown functions for both the electrochemical fields, $\psi_{\pm}^{\text{cl}}(X, t)$ and $C_{\pm}^{\text{cl}}(X, t)$. Specifically, $+$ denotes the functions in $X \in (h, h + d]$, whereas $-$ indicates the fields in $X \in [-h - d, -h)$. Furthermore, $\epsilon_{\pm}^{\text{cl}}$ and $\mathcal{D}_{\pm}^{\text{cl}}$ are the electric permittivities and diffusivities, and $\phi_{\pm}$ are the ionomer volume fractions in the CLs.

The IPMC manufacturing may in general lead to $\phi_+ \neq \phi_-$, as well as to different CL thicknesses $d_+ \neq d_-$. Any of these asymmetries leads to a non-symmetric electrochemical behaviour (with respect to the ionomer midplane $X = 0$). However, under the assumption of neglecting the electrochemical stresses in the linear momentum balance (generally holding in IPMC sensing [10] and here further discussed in Sections 5 and 6), the sole essential asymmetry in the properties needed to trigger a non-vanishing electrochemical response in compression sensing is the mechanical one, as explained in detail in [23] and adopted in the following. Given the uncertainties in IPMC manufacturing and the role played by the CL thicknesses and composition in the modelling, in our analytical development, for the sake of simplicity, we assume $d_+ = d_- \equiv d$, while we distinguish between ϕ_+ and ϕ_-.

2.1. Interface, boundary, and initial conditions

We complete the formulation of the compression sensing problem by imposing appropriate interface, boundary, and initial conditions.

At the ionomer-CL interfaces, we enforce the continuity of electric potential, counterions flux, and electric displacement through:

$$\psi(\pm h, t) = \psi_\pm^{\mathrm{cl}}(\pm h, t) \tag{2.7a}$$

$$J(\pm h, t) = J_\pm^{\mathrm{cl}}(\pm h, t) \tag{2.7b}$$

$$D(\pm h, t) = D_\pm^{\mathrm{cl}}(\pm h, t) \tag{2.7c}$$

According to [16], we adopt the following ionomer-CL interface condition for the counterions concentration:

$$C(\pm h, t) = \frac{C_\pm^{\mathrm{cl}}(\pm h, t)}{\phi_\pm} \tag{2.8}$$

which assumes that across each ionomer-CL interface the counterions concentration in the *plain* ionomer remains unaltered, and accounts for the fact that only a volume fraction $\phi_\pm$ of the CL is occupied by the ionomer.

By referring to Figure 1, at the CL-electrode interfaces we impose null electric potential due to the short-circuited electrodes, which are assumed to be perfect conductors:

$$\psi_\pm^{\mathrm{cl}}(\pm(h + d), t) = 0 \tag{2.9a}$$

Moreover, we apply the so-called *ion-blocking* condition, implying vanishing counterions flux at the electrodes:

$$J_\pm^{\mathrm{cl}}(\pm(h + d), t) = 0 \tag{2.9b}$$

Finally, we assume initial electroneutral state:

$$C(X, 0) = \frac{C_\pm^{\mathrm{cl}}(X, 0)}{\phi_\pm} = C_0 \tag{2.10a}$$

$$\psi(X, 0) = \psi_\pm^{\mathrm{cl}}(X, 0) = 0 \tag{2.10b}$$

2.2. Nondimensional governing equations

Suitably rewriting the governing equations in a nondimensional form is a crucial step to unveil the peculiar mathematical features of the IPMC sensing problem and analytically solve it by asymptotic analysis. To this aim, we introduce the following nondimensional variables:

$$\bar{X} = X/h, \quad \bar{u} = u/h, \quad \bar{C} = C/C_0, \quad \bar{\psi} = \psi/V_{\mathrm{th}}, \quad \bar{t} = t/\tau_0$$

where

$$V_{\mathrm{th}} = \frac{\mathcal{R}\mathcal{T}}{\mathcal{F}} \quad \text{and} \quad \tau_0 = \frac{h}{\mathcal{F}\mathcal{D}}\sqrt{\frac{\epsilon\mathcal{R}\mathcal{T}}{C_0}}$$

are the thermal voltage and the counterions characteristic diffusion time [6]. We note that, in studying IPMC sensing, the linearisation in (2.1) of the modified PNP system may lead to accurate results if the

applied displacement causes a voltage drop across the electrodes that is significantly smaller than V_{th}, whose value at room temperature is ≈ 25 mV.

Substituting the nondimensional variables in the governing equations (2.1) leads to

$$-\delta^2 \frac{\partial^2 \bar{\psi}(\bar{X}, \bar{t})}{\partial \bar{X}^2} = \bar{C}(\bar{X}, \bar{t}) - 1 \tag{2.11a}$$

$$\delta \left(\frac{\partial^2 \bar{C}(\bar{X}, \bar{t})}{\partial \bar{X}^2} + \frac{\partial^2 \bar{\psi}(\bar{X}, \bar{t})}{\partial \bar{X}^2} + \frac{1}{\nu - 1} \frac{\partial^3 \bar{u}(\bar{X}, \bar{t})}{\partial \bar{X}^3} \right) = \frac{\partial \bar{C}(\bar{X}, \bar{t})}{\partial \bar{t}} \tag{2.11b}$$

in which

$$\delta = \frac{1}{\mathcal{F} h} \sqrt{\frac{\epsilon \mathcal{R} \mathcal{T}}{C_0}} = \frac{\lambda_{\text{D}}}{h} \tag{2.12}$$

is a nondimensional positive parameter, proportional to the Debye screening length λ_{D} through the membrane semi-thickness h. In typical IPMCs, δ is very small ($\delta \approx 10^{-6}$ to 10^{-4} [28]), and this is a key point for the following asymptotic analysis [6].

In the CLs, we scale the counterions concentration in such a way that its nondimensional form assumes the same value of $\bar{C}$ at the ionomer-CL interfaces:

$$\bar{C}_{\pm}^{\text{cl}} = \frac{C_{\pm}^{\text{cl}}}{C_0 \phi_{\pm}} \tag{2.13}$$

Thus, Eqs (2.5) may be rewritten as

$$-\frac{\epsilon_{\pm}^{\text{cl}} \delta^2}{\epsilon \phi_{\pm}} \frac{\partial^2 \bar{\psi}_{\pm}^{\text{cl}}(\bar{X}, \bar{t})}{\partial \bar{X}^2} = \bar{C}_{\pm}^{\text{cl}}(\bar{X}, \bar{t}) - 1 \tag{2.14a}$$

$$\frac{\mathcal{D}_{\pm}^{\text{cl}} \delta}{\mathcal{D}} \left(\frac{\partial^2 \bar{C}_{\pm}^{\text{cl}}(\bar{X}, \bar{t})}{\partial \bar{X}^2} + \frac{\partial^2 \bar{\psi}_{\pm}^{\text{cl}}(\bar{X}, \bar{t})}{\partial \bar{X}^2} + \frac{1}{\nu - 1} \frac{\partial^3 \bar{u}(\bar{X}, \bar{t})}{\partial \bar{X}^3} \right) = \frac{\partial \bar{C}_{\pm}^{\text{cl}}(\bar{X}, \bar{t})}{\partial \bar{t}} \tag{2.14b}$$

We now specify the fundamental assumption on the relation between the CL and membrane bulk thicknesses, generally stating that $d \ll h$. To this purpose, we follow [16, 17] and further prescribe that d^2 is on the order of $\lambda_{\text{D}} h$. Given that $\lambda_{\text{D}} \ll h$, the CL turns out to be much wider than the Debye screening length and much thinner than the membrane bulk. By using Eq (2.12), this implies

$$d \propto h \sqrt{\delta}$$

Since we aim at analytically solving the problem by using the method of matched asymptotic expansions [26], we need to *suitably* magnify the CL regions. Hence, we introduce the following nondimensional spatial variables:

$$r_{\pm} = \frac{1 + \dfrac{d}{h} \mp \bar{X}}{\sqrt{\delta}} \tag{2.15}$$

The governing equations (2.14) are then conveniently rewritten as follows:

$$-\epsilon_{\pm}^* \frac{\partial^2 \bar{\psi}_{\pm}^{\text{cl}}(r_{\pm}, \bar{t})}{\partial (r_{\pm})^2} = \bar{C}_{\pm}^{\text{cl}}(r_{\pm}, \bar{t}) - 1 \tag{2.16a}$$

$$\mathcal{D}_\pm^* \delta \left(\frac{\partial^2 \bar{C}_\pm^{\mathrm{cl}}(r_\pm, \bar{t})}{\partial (r_\pm)^2} + \frac{\partial^2 \bar{\psi}_\pm^{\mathrm{cl}}(r_\pm, \bar{t})}{\partial (r_\pm)^2} + \frac{\delta}{\nu - 1} \frac{\partial^3 \bar{u}}{\partial \bar{X}^3} \bigg|_{\bar{X} = \mp (\sqrt{\delta} r_\pm - 1 - d/h)} \right) = \frac{\partial \bar{C}_\pm^{\mathrm{cl}}(r^\pm, \bar{t})}{\partial \bar{t}} \tag{2.16b}$$

Note that we do not express the third contribution at the left-hand side as a function of $r_\pm$ because the displacement is a known function of X. The same will hold in Sections 3.1.2, 3.1.4, and 3.1.5 where we need to rewrite the modified PNP system in terms of further local variables in order to obtain the solution in the boundary layers. Moreover, in Eqs (2.16), the electrochemical parameters

$$\epsilon_\pm^* = \frac{\epsilon_\pm^{\mathrm{cl}} \delta}{\epsilon \phi_\pm} \tag{2.17a}$$

$$\mathcal{D}_\pm^* = \frac{\mathcal{D}_\pm^{\mathrm{cl}}}{\mathcal{D} \delta} \tag{2.17b}$$

are assumed to be on the order of unit, or, less restrictively, they must have magnitudes such that the asymptotic solution of (2.16) is governed by δ. Mathematically, this gives restrictions to our model on how much larger and smaller the permittivity and the diffusivity of the CLs may be with respect to those of the plain ionomer. Physically, it of course means that the effect of metal particles within the composite layers is very relevant. The precise ranges of variation to be allowed for $\epsilon_\pm^*$ and $\mathcal{D}_\pm^*$ in order to obtain reliable predictions by using our novel analytical solution could be ascertained by a systematic comparison with the results of the fully coupled electrochemomechanical problem, as here accomplished in Section 5 to unveil other features of the analytical solution.

We remark that in order to solve the systems (2.11) and (2.14) within the boundary layers through the method of matched asymptotic expansions, in Sections 3.1.2, 3.1.4, and 3.1.5, we will introduce further spatial independent variables amplifying X and $r_\pm$ through δ and $\sqrt{\delta}$, respectively.

By referring to the coordinate $r_\pm$ as defined in (2.15), we indicate the nondimensional position of the ionomer-CL interfaces as

$$d^* = \frac{d}{h \sqrt{\delta}}$$

which corresponds to $\bar{X} = \pm 1$. Therefore, the nondimensional ionomer-CL interface conditions read

$$\bar{\psi}(\pm 1, \bar{t}) = \bar{\psi}_\pm^{\mathrm{cl}}(d^*, \bar{t}) \tag{2.18a}$$

$$\bar{J}(\pm 1, \bar{t}) = \bar{J}_\pm^{\mathrm{cl}}(d^*, \bar{t}) \tag{2.18b}$$

$$\bar{D}(\pm 1, \bar{t}) = \bar{D}_\pm^{\mathrm{cl}}(d^*, \bar{t}) \tag{2.18c}$$

$$\bar{C}(\pm 1, \bar{t}) = \bar{C}_\pm^{\mathrm{cl}}(d^*, \bar{t}) \tag{2.18d}$$

Finally, the nondimensional boundary and initial conditions are respectively rewritten as

$$\bar{\psi}_\pm^{\mathrm{cl}}(0, \bar{t}) = 0 \tag{2.19a}$$

$$\bar{J}_\pm^{\mathrm{cl}}(0, \bar{t}) = 0 \tag{2.19b}$$

and

$$\bar{C}(\bar{X}, 0) = \bar{C}_\pm^{\mathrm{cl}}(r_\pm, 0) = 1 \tag{2.20a}$$

$$\bar{\psi}(\bar{X}, 0) = \bar{\psi}_\pm^{\mathrm{cl}}(r_\pm, 0) = 0 \tag{2.20b}$$

3. Analytical solution by the method of matched asymptotic expansions

The modified PNP systems (2.11) and (2.16) represent characteristic perturbative problems [6], ruled by the small positive parameter δ. This class of mathematical problems can be conveniently solved by resorting to the method of matched asymptotic expansions [26], which consists of matching asymptotic solutions that hold in properly scaled regions of interest. In particular, we refer to:

- the *inner* regions, in the case at hand located near both the ionomer-CL and the CL-electrode interfaces, in which boundary layers may develop such that the solution should be subject to large gradients. We note that two inner solutions are needed for each ionomer-CL interface: One for system (2.11) in the ionomer close to the interface (Section 3.1.2), one for system (2.16) in the CL close to the interface (Section 3.1.4);
- the *outer* regions, here concerned with both the membrane bulk and each CL, whose points should be far enough from the interfaces (i.e., at a distance suitably larger than the Debye screening length from any interface). In the outer regions the solution is free from the large gradients characterising the boundary layers.

In the following, we first present the asymptotic expansions employed to solve the governing PDEs in each region (Section 3.1), then, we impose the conditions to match the obtained solutions (Section 3.2), and, finally, we provide the overall solution (in literature, also referred to as the "composite" solution), that is the solution holding in the entire domain (Section 3.3). Henceforth, in order to simplify the notation, we drop the overline denoting dimensionless quantities, unless otherwise specified.

3.1. Inner and outer expansions

3.1.1. Outer expansion in the ionomer

In this region, the field variables are free from large gradients, such that we directly substitute in the nondimensional system (2.11) the following regular outer expansions in the powers of δ, denoted with the superscript ^{o}:

$$C^o(X,t) = C^o_0(X,t) + \delta C^o_1(X,t) + \delta^2 C^o_2(X,t) + ... \tag{3.1a}$$

$$\psi^o(X,t) = \psi^o_0(X,t) + \delta\psi^o_1(X,t) + \delta^2\psi^o_2(X,t) + ... \tag{3.1b}$$

At the leading order, the solution of (2.11) turns out to be

$$C^o_0(X,t) = 1 \tag{3.2a}$$

$$\psi^o_0(X,t) = \frac{1}{1-\nu}\frac{\partial u(X,t)}{\partial X} + A_1(t)X + A_2(t) \tag{3.2b}$$

Here and henceforth, A_i and B_i (with $i = 1, 2, 3, \ldots$) are unknown functions of time that have to be determined by applying matching, interface, and boundary conditions.

3.1.2. Inner expansions in the ionomer

In order to capture the behaviour of the relevant field variables in the boundary layers, we magnify the interface regions, by properly scaling the spatial variable X into the local variables ξ^+ and ξ^-:

$$\xi^\pm = \frac{1 \mp X}{\delta} \tag{3.3}$$

Equations (2.11) then become

$$-\frac{\partial^2 \psi^\pm(\xi^\pm, t)}{\partial(\xi^\pm)^2} = C^\pm(\xi^\pm, t) - 1 \tag{3.4a}$$

$$\frac{\partial^2 C^\pm(\xi^\pm, t)}{\partial(\xi^\pm)^2} + \frac{\partial^2 \psi^\pm(\xi^\pm, t)}{\partial(\xi^\pm)^2} + \delta^2 \frac{1}{\nu - 1} \frac{\partial^3 u(X, t)}{\partial X^3}\bigg|_{X=\mp(\delta\xi^\pm - 1)} = \delta \frac{\partial C^\pm(\xi^\pm, t)}{\partial t} \tag{3.4b}$$

By following the notation of [17], *in the boundary layers* we always use the superscripts $+$ and $-$ to indicate the field variables at the ionomer-CL interfaces at $X = 1$ and at $X = -1$, respectively. Moreover, we employ $\pm$ as superscript, as in Eq (3.3) for ξ, to indicate the local variables in the boundary layers, whereas we employ $\pm$ as subscript, as in Eq (2.15) for r, to denote the local variables in the CLs.

System (3.4) can be solved by substitution of regular inner expansions (denoted with the superscripts $\pm$):

$$C^\pm(\xi^\pm, t) = C_0^\pm(\xi^\pm, t) + \delta C_1^\pm(\xi^\pm, t) + \delta^2 C_2^\pm(\xi^\pm, t) + ... \tag{3.5a}$$

$$\psi^\pm(\xi^\pm, t) = \psi_0^\pm(\xi^\pm, t) + \delta\psi_1^\pm(\xi^\pm, t) + \delta^2\psi_2^\pm(\xi^\pm, t) + ... \tag{3.5b}$$

thus obtaining, at the leading order, the general *bounded* solution [23]:

$$C^\pm(\xi^\pm, t) \approx C_0^\pm(\xi^\pm, t) = 1 - A_3^\pm(t)e^{-\xi^\pm} \tag{3.6a}$$

$$\psi^\pm(\xi^\pm, t) \approx \psi_0^\pm(\xi^\pm, t) = A_3^\pm(t)e^{-\xi^\pm} + A_4^\pm(t) \tag{3.6b}$$

in which we disregard the contributions involving $\xi^\pm$ and $e^{\xi^\pm}$ because the solution must be bounded for $\xi^\pm \to \infty$, that is where (3.6) must match the outer solution (3.2) (see Section 3.2).

3.1.3. Outer expansions in the CLs

By referring to Eqs (2.16), in the CLs we adopt the following asymptotic expansions:

$$C_{\text{cl}\pm}^o(r_\pm, t) = C_{\text{cl}0\pm}^o(r_\pm, t) + \sqrt{\delta} C_{\text{cl}1\pm}^o(r_\pm, t) + ... \tag{3.7a}$$

$$\psi_{\text{cl}\pm}^o(r_\pm, t) = \psi_{\text{cl}0\pm}^o(r_\pm, t) + \sqrt{\delta}\psi_{\text{cl}1\pm}^o(r_\pm, t) + ... \tag{3.7b}$$

By substituting Eqs (3.7) in the system (2.16), and by referring to the initial condition (2.20a), we find the following solution at the leading order:

$$C_{\text{cl}0\pm}^o(r_\pm, t) = 1 \tag{3.8a}$$

$$\psi_{\text{cl}0\pm}^o(r_\pm, t) = B_1^\pm(t)r_\pm + B_2^\pm(t) \tag{3.8b}$$

3.1.4. Inner expansions in the CLs: interfaces with the ionomer

In these boundary layer regions, in order to obtain the solution of system (2.16), we magnify the domain by introducing the local variables

$$\eta^\pm = \frac{d^* - r_\pm}{\sqrt{\delta}} \tag{3.9}$$

Note that the local variables $r_\pm$ and $\eta^\pm$ are defined in such a way that the two ionomer-CL interfaces turn out to be both located at d^* or 0 depending on whether they are identified by $r_\pm$ or $\eta^\pm$ (see also Eq (2.15)).

Substitution of (3.9) in system (2.16) leads to

$$-\epsilon_\pm^* \frac{\partial^2 \psi_{cl\pm}^\pm(\eta^\pm, t)}{\partial(\eta^\pm)^2} = \delta\left(C_{cl\pm}^\pm(\eta^\pm, t) - 1\right) \tag{3.10a}$$

$$\mathcal{D}_\pm^*\left(\frac{\partial^2 C_{cl\pm}^\pm(\eta^\pm, t)}{\partial(\eta^\pm)^2} + \frac{\partial^2 \psi_{cl\pm}^\pm(\eta^\pm, t)}{\partial(\eta^\pm)^2} + \frac{\delta^2}{\nu - 1}\frac{\partial^3 u}{\partial X^3}\bigg|_{X=\pm\left(\delta\eta^\pm - \sqrt{\delta}d^* + 1 + d/h\right)}\right) = \frac{\partial C_{cl\pm}^\pm(\eta^\pm, t)}{\partial t} \tag{3.10b}$$

This system is conveniently solved by using the regular asymptotic expansions

$$C_{cl\pm}^\pm(\eta^\pm, t) = C_{cl0\pm}^\pm(\eta^\pm, t) + \sqrt{\delta}C_{cl1\pm}^\pm(\eta^\pm, t) + \dots \tag{3.11a}$$

$$\psi_{cl\pm}^\pm(\eta^\pm, t) = \psi_{cl0\pm}^\pm(\eta^\pm, t) + \sqrt{\delta}\psi_{cl1\pm}^\pm(\eta^\pm, t) + \dots \tag{3.11b}$$

Hence, at the leading order, system (3.10) becomes

$$\frac{\partial^2 \psi_{cl0\pm}^\pm(\eta^\pm, t)}{\partial(\eta^\pm)^2} = 0 \tag{3.12a}$$

$$\frac{\partial C_{cl0\pm}^\pm(\eta^\pm, t)}{\partial t} = \mathcal{D}_\pm^* \frac{\partial^2 C_{cl0\pm}^\pm(\eta^\pm, t)}{\partial(\eta^\pm)^2} \tag{3.12b}$$

The general solution of Eq (3.12a) is

$$\psi_{cl0\pm}^\pm(\eta^\pm, t) = B_3^\pm(t)\eta^\pm + B_4^\pm(t) \tag{3.13}$$

while expressions (3.12b) represent diffusion equations [29] requiring further conditions that we establish in Section 3.2.

3.1.5. Inner expansions in the CLs: interfaces with the electrodes

According to the foregoing approach, we introduce the local variables

$$\zeta^\pm = \frac{r_\pm}{\sqrt{\delta}} \tag{3.14}$$

whose substitution in system (2.16) leads to the following governing system:

$$-\epsilon_\pm^* \frac{\partial^2 \psi_{cl0\pm}^\mp(\zeta^\pm, t)}{\partial(\zeta^\pm)^2} = \delta\left(C_{cl0\pm}^\mp(\zeta^\pm, t) - 1\right) \tag{3.15a}$$

$$\mathcal{D}_\pm^*\left(\frac{\partial^2 C_{cl0\pm}^\mp(\zeta^\pm, t)}{\partial(\zeta^\pm)^2} + \frac{\partial^2 \psi_{cl0\pm}^\mp(\zeta^\pm, t)}{\partial(\zeta^\pm)^2} + \frac{\delta^2}{\nu - 1}\frac{\partial^3 u}{\partial X^3}\bigg|_{X=\mp(\delta\zeta^\pm - 1 - d/h)}\right) = \frac{\partial C_{cl0\pm}^\mp(\zeta^\pm, t)}{\partial t} \tag{3.15b}$$

At the leading order it becomes

$$\frac{\partial^2 \psi_{cl0\pm}^\mp(\zeta^\pm, t)}{\partial(\zeta^\pm)^2} = 0 \tag{3.16a}$$

$$\frac{\partial C_{\text{cl0}\pm}^{\mp}(\zeta^{\pm}, t)}{\partial t} = \mathcal{D}_{\pm}^{*} \frac{\partial^2 C_{\text{cl0}\pm}^{\mp}(\zeta^{\pm}, t)}{\partial(\zeta^{\pm})^2} \tag{3.16b}$$

Note that here the superscripts $+$ and $-$ indicate the CL-electrode interfaces at $r_- = 0$ ($\zeta_- = 0$) and $r_+ = 0$ ($\zeta_+ = 0$), respectively.

The general solution of (3.16a) is

$$\psi_{\text{cl0}\pm}^{\mp}(\zeta^{\pm}, t) = B_5^{\pm}(t)\zeta^{\pm} + B_6^{\pm}(t) \tag{3.17}$$

while the diffusion equations (3.16b), as well as (3.12b), are solved next, in Section 3.2.

3.2. Matching conditions and problem solution

The matching conditions consist of the following limit conditions, through which the outer and inner solutions, at the leading order, are related in this asymptotic analysis [26]:

$$\lim_{\xi^{\pm} \to \infty} C_0^{\pm}(\xi^{\pm}, t) = \lim_{X \to \pm 1} C_0^{o}(X, t) \tag{3.18a}$$

$$\lim_{\xi^{\pm} \to \infty} \psi_0^{\pm}(\xi^{\pm}, t) = \lim_{X \to \pm 1} \psi_0^{o}(X, t) \tag{3.18b}$$

$$\lim_{\eta^{\pm} \to \infty} C_{\text{cl0}\pm}^{\pm}(\eta^{\pm}, t) = \lim_{r_{\pm} \to d^*} C_{\text{cl0}\pm}^{o}(r_{\pm}, t) \tag{3.18c}$$

$$\lim_{\eta^{\pm} \to \infty} \psi_{\text{cl0}\pm}^{\pm}(\eta^{\pm}, t) = \lim_{r_{\pm} \to d^*} \psi_{\text{cl0}\pm}^{o}(r_{\pm}, t) \tag{3.18d}$$

$$\lim_{\zeta^{\pm} \to \infty} C_{\text{cl0}\pm}^{\mp}(\zeta^{\pm}, t) = \lim_{r_{\pm} \to 0} C_{\text{cl0}\pm}^{o}(r_{\pm}, t) \tag{3.18e}$$

$$\lim_{\zeta^{\pm} \to \infty} \psi_{\text{cl0}\pm}^{\mp}(\zeta^{\pm}, t) = \lim_{r_{\pm} \to 0} \psi_{\text{cl0}\pm}^{o}(r_{\pm}, t) \tag{3.18f}$$

Condition (3.18a) is trivially satisfied, whereas the application of (3.18b), (3.18d), and (3.18f) leads to

$$A_4^{\pm}(t) = \frac{1}{1-\nu} \left.\frac{\partial u(X, t)}{\partial X}\right|_{X=\pm 1} \pm A_1(t) + A_2(t) \tag{3.19a}$$

$$B_3^{\pm}(t) = 0, \quad B_4^{\pm}(t) = B_1^{\pm}(t)d^* + B_2^{\pm}(t) \tag{3.19b}$$

$$B_5^{\pm}(t) = 0, \quad B_6^{\pm}(t) = B_2^{\pm}(t) \tag{3.19c}$$

By using the boundary condition (2.19a) in (3.17), and then condition (3.19c), we obtain

$$B_6^{\pm}(t) = 0 \quad \Rightarrow \quad B_2^{\pm}(t) = 0 \tag{3.20}$$

Combination of (2.19b) and (3.15b) with the initial condition (2.20a) leads to

$$C_{\text{cl0}\pm}^{\mp}(0, t) = 1 \tag{3.21}$$

which is the counterions concentration at the CL-electrode interfaces. By referring to the classical theory of diffusion equations [29], we employ conditions (3.21) and (3.18e) to solve Eq (3.16b), thus obtaining

$$C_{\text{cl0}\pm}^{\mp}(\zeta^{\pm}, t) = 1 \tag{3.22}$$

Similarly, we use the interface condition (2.18d) and the matching condition (3.18c) to determine

$$C_{\text{cl}0\pm}^{\pm}(0, t) = 1 - A_3^{\pm}(t) \tag{3.23a}$$

$$\lim_{\eta^{\pm} \to \infty} C_{\text{cl}0\pm}^{\pm}(\eta^{\pm}, t) = 1 \tag{3.23b}$$

such that, as classical in diffusion equations, we solve (3.12b) by expressing the counterions concentrations close to the ionomer-CL interfaces through the complementary error function erfc:

$$C_{\text{cl}0\pm}^{\pm}(\eta^{\pm}, t) = 1 - \int_0^t \frac{dA_3^{\pm}(k)}{dk} \, \text{erfc}\left(\frac{\eta^{\pm}}{\sqrt{4\mathcal{D}_{\pm}^*(t - k)}}\right) dk \tag{3.24}$$

where k acts as a dummy variable.

Finally, the interface condition (2.18a) leads to

$$A_3^{\pm}(t) + A_4^{\pm}(t) = B_4^{\pm}(t) \tag{3.25}$$

In order to complete the problem formulation and determine the remaining unknown functions of time entering the foregoing general solutions, we first evaluate the rate of change of the charge stored at the ionomer-CL interfaces by integrating Eq (2.11b):

$$\int_{\pm 1}^{X} \frac{\partial C(X', t)}{\partial t} dX' = \delta\left(\frac{\partial C(X, t)}{\partial X} + \frac{\partial \psi(X, t)}{\partial X} + \frac{1}{\nu - 1}\frac{\partial^2 u(X, t)}{\partial X^2}\right)$$
$$- \delta\left(\frac{\partial C(X, t)}{\partial X}\bigg|_{X=\pm 1} + \frac{\partial \psi(X, t)}{\partial X}\bigg|_{X=\pm 1} + \frac{1}{\nu - 1}\frac{\partial^2 u(X, t)}{\partial X^2}\bigg|_{X=\pm 1}\right) \tag{3.26}$$

where X' is a dummy variable. Then, after moving the second term at the right-hand side of (3.26) to the left-hand side, we specialise the left-hand side to the inner solution and the right-hand side to the outer solution:

$$\mp \int_0^{\infty} \frac{\partial C^{\pm}(\xi'^{\pm}, t)}{\partial t} d\xi'^{\pm} + \frac{1}{\delta}\left(\mp \frac{\partial C^{\pm}(\xi^{\pm}, t)}{\partial \xi^{\pm}}\bigg|_{\xi^{\pm}=0} \mp \frac{\partial \psi^{\pm}(\xi^{\pm}, t)}{\partial \xi^{\pm}}\bigg|_{\xi^{\pm}=0} + \frac{\delta}{\nu - 1}\frac{\partial^2 u(X, t)}{\partial X^2}\bigg|_{X=\pm 1}\right)$$
$$= \lim_{X \to \pm 1}\left(\frac{\partial C^o(X, t)}{\partial X} + \frac{\partial \psi^o(X, t)}{\partial X} + \frac{1}{\nu - 1}\frac{\partial^2 u(X, t)}{\partial X^2}\bigg|_{X=\pm 1}\right) \tag{3.27}$$

Now, we first evaluate the first addend at the left-hand side by solving Eq (3.4a), at the leading order, for $C_0^{\pm}$. Second, to take the limit for $\delta \to 0$ we apply the continuity condition of the ion flux at the ionomer-CL interfaces (2.18b), which, after scaling by $\mathcal{D}C_0/h$, can be rewritten as

$$\frac{1}{\delta}\left(\mp \frac{\partial C^{\pm}(0, t)}{\partial \xi^{\pm}} \mp \frac{\partial \psi^{\pm}(0, t)}{\partial \xi^{\pm}} + \delta\frac{1}{\nu - 1}\frac{\partial^2 u(X, t)}{\partial X^2}\bigg|_{X=\pm 1}\right)$$
$$= \mathcal{D}_{\pm}^*\phi_{\pm}\left(\pm \frac{\partial C_{\text{cl}0\pm}^{\pm}(0, t)}{\partial \eta^{\pm}} \pm \frac{\partial \psi_{\text{cl}0\pm}^{\pm}(0, t)}{\partial \eta^{\pm}} + \delta\frac{1}{\nu - 1}\frac{\partial^2 u(X, t)}{\partial X^2}\bigg|_{X=\pm(-d^*+1+d/h)}\right) \tag{3.28}$$

Third, we substitute the outer solution (3.2) in the right-hand side of Eq (3.27), such that condition (3.27) becomes

$$\mp \frac{\partial^2 \psi_0^{\pm}(0, t)}{\partial \xi^{\pm}\partial t} \pm \mathcal{D}_{\pm}^*\phi_{\pm}\left(\frac{\partial C_{\text{cl}0\pm}^{\pm}(0, t)}{\partial \eta^{\pm}} + \frac{\partial \psi_{\text{cl}0\pm}^{\pm}(0, t)}{\partial \eta^{\pm}}\right) = A_1(t) \tag{3.29}$$

We substitute in the left-hand side of Eq (3.29) the inner solutions (3.6b), (3.24) and (3.13) (along with condition (3.19b)), holding in the ionomer and in the CLs, respectively, to finally obtain

$$\pm \frac{\mathrm{d}A_3^\pm(t)}{\mathrm{d}t} \pm \sqrt{\frac{\mathcal{D}_\pm^* \phi_\pm^2}{\pi}} \int_0^t \frac{1}{\sqrt{t-k}} \frac{\mathrm{d}A_3^\pm(k)}{\mathrm{d}k} \mathrm{d}k = A_1(t) \tag{3.30}$$

which has to be integrated by using the initial condition

$$A_3^\pm(0) = 0 \tag{3.31}$$

We now proceed by enforcing the continuity of the electric displacement (2.18c). To this purpose, we evaluate the charge density in each CL near the interface, by integrating Eq (2.16a):

$$-\epsilon_\pm^* \left[\frac{\partial \psi_\pm^{\mathrm{cl}}(r_\pm, t)}{\partial r_\pm} - \frac{\partial \psi_\pm^{\mathrm{cl}}(d^*, t)}{\partial r_\pm} \right] = \int_{d^*}^{r_\pm} \left(C_\pm^{\mathrm{cl}}(r', t) - 1 \right) \mathrm{d}r' \tag{3.32}$$

where r' is a dummy variable. Then, after moving the second term at the left-hand side to the right-hand side, we use the outer solution (3.8b) to evaluate the left-hand side and we rewrite the right-hand side in terms of the inner solutions in the CLs. At the leading order, we obtain

$$\epsilon_\pm^* B_1^\pm(t) = \sqrt{\delta} \int_0^\infty \left(C_{\mathrm{cl}0\pm}^\pm(\eta^\pm, t) - 1 \right) \mathrm{d}\eta^\pm - \epsilon_\pm^* \frac{\partial \psi_{\mathrm{cl}0\pm}^\pm(0, t)}{\partial \eta^\pm} \frac{1}{\sqrt{\delta}} \tag{3.33}$$

We can now write the right-hand side of Eq (3.33) in terms of $A_3^\pm(t)$. By substituting Eq (3.24) in the first term at the right-hand side of Eq (3.33) we obtain

$$\sqrt{\delta} \int_0^\infty \left(C_{\mathrm{cl}0\pm}^\pm(\eta^\pm, t) - 1 \right) \mathrm{d}\eta^\pm = -\sqrt{\delta} \int_0^t \frac{\mathrm{d}A_3^\pm(k)}{\mathrm{d}k} \frac{\sqrt{4\mathcal{D}_\pm^*(t-k)}}{\sqrt{\pi}} \mathrm{d}k \tag{3.34}$$

Moreover, to remove the singularity for $\delta \to 0$ in Eq (3.33), we use the interface condition on the electric displacement (2.18c), which, after scaling by $\epsilon V_{\mathrm{th}}/h$, can be rewritten as

$$\pm \frac{\epsilon}{\delta} \frac{\partial \psi_0^\pm(0, t)}{\partial \xi^\pm} = \mp \frac{\epsilon_{\mathrm{cl}}}{\delta} \frac{\partial \psi_{\mathrm{cl}0\pm}^\pm(0, t)}{\partial \eta^\pm} \tag{3.35}$$

Hence, by referring to Eqs (2.17a) and (3.6b), the second term at the right-hand side of Eq (3.33) becomes

$$\frac{\epsilon_\pm^*}{\sqrt{\delta}} \frac{\partial \psi_{\mathrm{cl}0\pm}^\pm(0, t)}{\partial \eta^\pm} = \frac{\sqrt{\delta}}{\phi_\pm} A_3^\pm(t) \tag{3.36}$$

Finally, by substituting Eqs (3.34) and (3.36) in Eq (3.33), we find

$$\epsilon_\pm^* B_1^\pm(t) = -\sqrt{\delta} \int_0^t \frac{\mathrm{d}A_3^\pm(k)}{\mathrm{d}k} \frac{\sqrt{4\mathcal{D}_\pm^*(t-k)}}{\sqrt{\pi}} \mathrm{d}k - \frac{\sqrt{\delta}}{\phi_\pm} A_3^\pm(t) \tag{3.37}$$

The foregoing procedure closes the problem, in which the ten unknown functions

$$A_1(t), \quad A_2(t), \quad A_3^\pm(t), \quad A_4^\pm(t), \quad B_1^\pm(t), \quad B_4^\pm(t)$$

must be determined by solving Eqs (3.19a), (3.19b), (3.25), (3.30), and (3.37).

Specifically, we solve the differential equations (3.30) by adopting the unilateral Laplace transform $\mathcal{L}[\cdot]$, thus obtaining

$$\mathcal{L}[A_3^+](s) = -\mathcal{L}[A_3^-](s) = \mathcal{L}[A_3](s) \quad \Rightarrow \quad \mathcal{L}[A_3](s)\left(s + \sqrt{\mathcal{D}_\pm^* \, \phi_\pm^2} \, \sqrt{s}\right) = \mathcal{L}[A_1](s) \tag{3.38a}$$

where s is the nondimensional Laplace variable. Then, relations (3.37), (3.19b), (3.25), and (3.19a) may be finally reformulated by straightforwardly eliminating four unknowns as follows:

$$\mathcal{L}[B_1^+](s) = -\mathcal{L}[B_1^-](s) = \mathcal{L}[B_1](s) \quad \Rightarrow \quad \mathcal{L}[B_1](s) = -\frac{1}{\epsilon_\pm^*}\mathcal{L}[A_3](s)\left(\sqrt{\frac{\mathcal{D}_\pm^*\delta}{s}} + \sqrt{\frac{\delta}{\phi_\pm}}\right) \tag{3.38b}$$

$$\mathcal{L}[B_4^+](s) = -\mathcal{L}[B_4^-](s) = \mathcal{L}[B_4](s) \quad \Rightarrow \quad \mathcal{L}[B_4](s) = \mathcal{L}[B_1](s)d^* \tag{3.38c}$$

$$\mathcal{L}[A_4^+](s) = -\mathcal{L}[A_4^-](s) = \mathcal{L}[A_4](s) \quad \Rightarrow \quad \mathcal{L}[A_3](s) + \mathcal{L}[A_4](s) = \mathcal{L}[B_4](s) \tag{3.38d}$$

$$\mathcal{L}[A_4](s) = \frac{1}{1-\nu}\mathcal{L}\left[\left.\frac{\partial u(X, s)}{\partial X}\right|_{X=\pm 1}\right] \pm \mathcal{L}[A_1](s) + \mathcal{L}[A_2](s) \tag{3.38e}$$

Therefore, system (3.38) reduces the problem to six equations (note that (3.38e) includes two equations) in the Laplace domain to be solved for

$$\mathcal{L}[A_1](s), \quad \mathcal{L}[A_2](s), \quad \mathcal{L}[A_3](s), \quad \mathcal{L}[A_4](s), \quad \mathcal{L}[B_1](s), \quad \mathcal{L}[B_4](s)$$

3.3. Overall solution

As a final step, we combine the outer solutions and the inner solutions, by accounting for their common limits. This allows us to express the counterions concentration and the electric potential in the whole domain in terms of $\mathcal{L}[A_1](s), \mathcal{L}[A_2](s), \mathcal{L}[A_3](s)$, and $\mathcal{L}[B_1](s)$ to be obtained from system (3.38):

$$\mathcal{L}[C](X, s) = \frac{1}{s} - \mathcal{L}[A_3](s)\left[e^{(X-1)/\delta} - e^{(-X-1)/\delta}\right] \tag{3.39a}$$

$$\mathcal{L}[\psi](X, s) = \mathcal{L}[A_1](s)X + \mathcal{L}[A_2](s) + \frac{1}{1-\nu}\mathcal{L}\left[\frac{\partial u(X, s)}{\partial X}\right] + \mathcal{L}[A_3](s)\left[e^{(X-1)/\delta} - e^{(-X-1)/\delta}\right] \tag{3.39b}$$

$$\mathcal{L}[C_\pm^{\mathrm{cl}}](r_\pm, s) = \frac{1}{s} - \mathcal{L}[A_3](s)e^{-\left[(d^*-r_\pm)/\sqrt{\delta}\right]\sqrt{s/\mathcal{D}_\pm^*}} \tag{3.39c}$$

$$\mathcal{L}[\psi_\pm^{\mathrm{cl}}](r_\pm, s) = \mathcal{L}[B_1](s)r_\pm \tag{3.39d}$$

The final solution is established by numerical Laplace inversion.[*]

---

[*]To this purpose, we resort to a built-in function implementing the Piessens' method in the commercial software Mathematica [30].

3.4. Equivalent circuit model and qualitative discussion of the analytical solution

By referring to classical theories (see, e.g., [31]), the response of an electrochemical cell can be conveniently recast into an equivalent circuit. The class of sensing problems we deal with extends this conventional representation by accounting for the mechanics which enters the picture as a voltage source.

Here, we obtain an equivalent circuit model for the IPMC compression sensing directly from the overall solutions (3.39) by adapting the classical circuit with lumped components proposed by Randles [31]. The resulting circuit, displayed in Figure 2, is characterised by overall resistance, capacitance, and impedance (the latter being of the Warburg type, as established in the following).
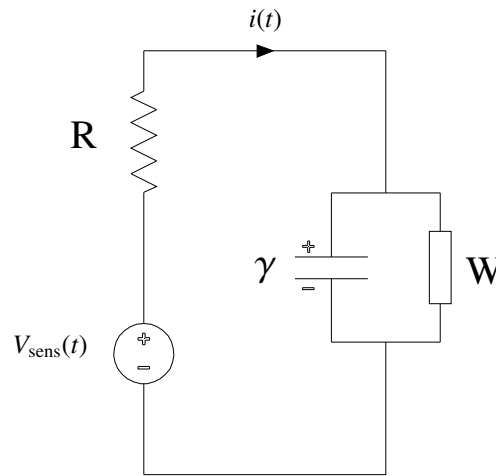

Figure 2. Equivalent circuit model, characterised by resistance R, capacitance γ, and Warburg impedance W, all evaluated per unit surface area. The voltage source $V_{\text{sens}}(t)$ due to compression leads to the electric current $i(t)$.

First, we determine the nondimensional short-circuit electric current flowing through the IPMC, evaluated at the ionomer-CL interfaces by referring to Eqs (2.4) and (2.6). Then, by comparison with (3.29), we obtain

$$i(t) = \pm \frac{\partial^2 \psi_0^\pm(0,t)}{\partial \xi^\pm \partial t} \mp \mathcal{D}_\pm^* \phi_\pm \left(\frac{\partial C_{\text{cl}0\pm}^\pm(0,t)}{\partial \eta^\pm} + \frac{\partial \psi_{\text{cl}0\pm}^\pm(0,t)}{\partial \eta^\pm} \right) = -A_1(t) \tag{3.40}$$

Second, by resorting to dimensional quantities and by referring to Eqs (3.2b) and (3.6b), we evaluate the voltage drop in the membrane bulk and in the boundary layer regions:

$$\Delta V_{\text{out}}(t) = \underbrace{2V_{\text{th}}A_1(t)}_{-\text{R}\,i(t)} + \underbrace{\frac{V_{\text{th}}}{1-\nu} \left(\left. \frac{\partial u(X,t)}{\partial X} \right|_{X=h} - \left. \frac{\partial u(X,t)}{\partial X} \right|_{X=-h} \right)}_{V_{\text{sens}}(t)} \tag{3.41a}$$

$$\Delta V^\pm(t) = V_{\text{th}}A_3(t) \tag{3.41b}$$

Note that $i(t)$ in Eq (3.40) is a nondimensional electric current, while $i(t)$ highlighted in Eq (3.41a) is the dimensional one, obtained through the scaling coefficient $\mathcal{F}\mathcal{D}C_0/h$. Hence, the resistance per unit

surface area results

$$\text{R} = \frac{2h\mathcal{RT}}{\mathcal{F}^2 \mathcal{D} C_0} \tag{3.42}$$

and the first contribution at the right-hand side of (3.41a) represents the voltage drop in the bulk. Moreover, in Eq (3.41a), the quantity $V_{\text{sens}}(t)$ is related to the displacement field in the ionomer, and can be interpreted as a lumped voltage source. Note that this term vanishes if the applied deformation field assumes the same value at the two ionomer-CL interfaces. Therefore, likewise the case neglecting CLs [23], an appropriate spatially non-uniform through-the-thickness elastic modulus is essential to obtain a sensing response for this benchmark within the adopted Cha and Porfiri [4] theory. One might expect less restrictive conditions when focusing on the *fully coupled* nonlinear problem, given the interaction, within the ionomer-CL interface regions, between the elastic modulus variation and possibly asymmetric gradients in the electrochemical properties. For instance, on the one hand, any gradient of elastic modulus can trigger a Fick's law-driven counterions flux, leading to an electric field contributing, through the polarisation (or Maxwell) stress, to the linear momentum balance. However, on the other hand, large permittivity and low diffusivity as those characterising the CLs should cause very low electric field. Hence, assessing the effectiveness of factors disregarded by the analytical solution (3.41a) in determining the actual sensing response would require a thorough investigation, also encompassing a detailed characterisation of the IPMC microstructure. In any case, an asymmetry in the IPMC properties, with respect to the midplane $X = 0$, is needed along with a gradient in the elastic modulus. Most likely, this may be ascribed to the differences, due to manufacturing, in the two CL regions, whose electrochemical properties modulate the observed electric current, as also clear from the definition below of the overall impedance in the analytical solution.

Under the fundamental assumption $d \ll h$, the short-circuit current (3.40) can be related to the voltage drop across the boundary layers (3.41b), directly associated with double-layer charging and Faradaic processes. In particular, the double-layer effect can be included in the equivalent circuit through a pure capacitance element, while the Faradaic processes related to mass transfer in the CLs are accounted for by introducing a Warburg impedance element. By combining the dimensional form of Eqs (3.38a) and (3.40) with (3.41b), we obtain a parallel connection between a capacitor of constant

$$\gamma = \frac{\mathcal{F}}{2} \sqrt{\frac{\epsilon C_0}{\mathcal{RT}}} \tag{3.43}$$

and a component of Warburg impedance

$$\text{W} = \frac{\mathcal{F}^2 C_0 \sqrt{\mathcal{D}^{\text{cl}}_{\pm} \phi^2_{\pm}}}{\mathcal{RT}} \tag{3.44}$$

Therefore, according to the scheme in Figure 2, the equivalent circuit has overall impedance, relating $i(t)$ to $V_{\text{sens}}(t)$, reading as follows in the Laplace domain:

$$\text{Z}(s) = \frac{1 + \text{RW}\sqrt{s} + \text{R}\gamma\, s}{\text{W}\sqrt{s} + \gamma\, s} \tag{3.45}$$

We finally remark that the present equivalent circuit model could be obtained by properly combining the circuits established in [16, 17] and [23], respectively for the plain electrochemistry with CLs (providing the Warburg impedance) and for compression sensing in the absence of CLs (providing the voltage source).

4. Validation of the analytical solution and general description of IPMC compression sensing

4.1. Particularisation to the case of ionomer with uniform electrochemical properties

To offer a first validation of the analytical solution developed in Section 3, here we focus on a specific case in which the profiles of concentration and electric potential described by the solutions (3.39) are expected to be comparable to those obtained for sensing without CLs [23]. This comparison is meaningful because of the large difference in complexity between the two analytical solutions. In particular, the solution neglecting CLs [23], which accounts for two boundary layers at the electrodes only, is totally explicit and does not require any Laplace transform. This comparison also offers us the opportunity to explain some notions on the IPMC sensing behaviour that are useful for the discussions in Sections 5 and 6.

We assume deformation-free CLs having similar properties to those of the electrodes. In particular, we set the volume fraction of the ionomer in the CLs close to zero ($\phi_\pm = 0.001$) and, with respect to the values on the order of unit as discussed about Eqs (2.17), we largely increase the CL permittivity ($\epsilon_\pm^* = 1000$) and decrease the CL diffusivity ($\mathcal{D}_\pm^* = 0.001$).

For what concerns the ionomer, we consider the IPMC data reported in Table 1 of [23]. In particular, the chosen asymmetric elastic modulus leads to the applied deformation field in the membrane bulk displayed in Figure 3.

The compressive displacement applied at the top face linearly increases in time, reaching the peak value $\hat{u}(t_f) = 5\ \mu$m at the final instant $t_f = 0.5$ ms.
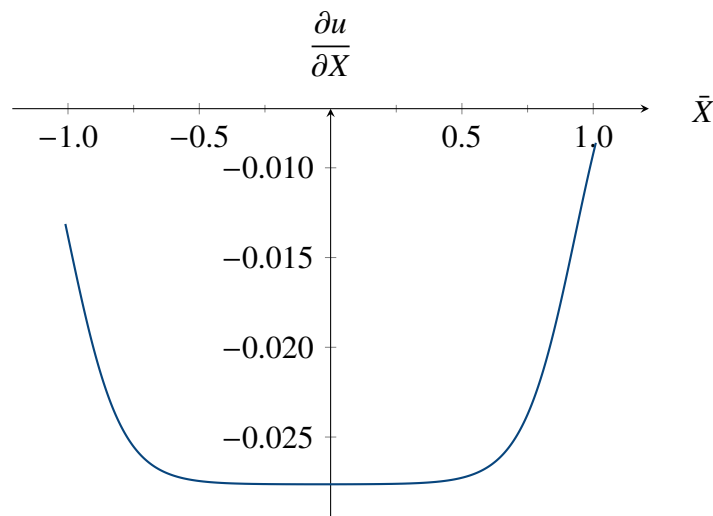

Figure 3. Profile of imposed deformation along the ionomer thickness [23].

Figure 4 illustrates the perfect match in the comparison between the results obtained with the new solution and those of [23]. Delving into some detail of the IPMC sensing behaviour, Figure 4a shows the counterions concentration along the membrane thickness at the end of the analysis, $t_f = 0.5$ ms. Except for the interface regions, the concentration profile is basically uniform, remaining unaltered with respect to the initial concentration $C_0 = 1200$ mol/m^3. At the two interfaces, boundary layers develop and the profile shows narrow peaks of approximately the same magnitude and opposite sign.

The counterions concentration reaches the values $C(-h, t_f) = 1198.591$ mol/m^3 and $C(h, t_f) = 1201.409$ mol/m^3 in [23] against the values $C(-h, t_f) = 1198.596$ mol/m^3 and $C(h, t_f) = 1201.405$ mol/m^3 in the present model.
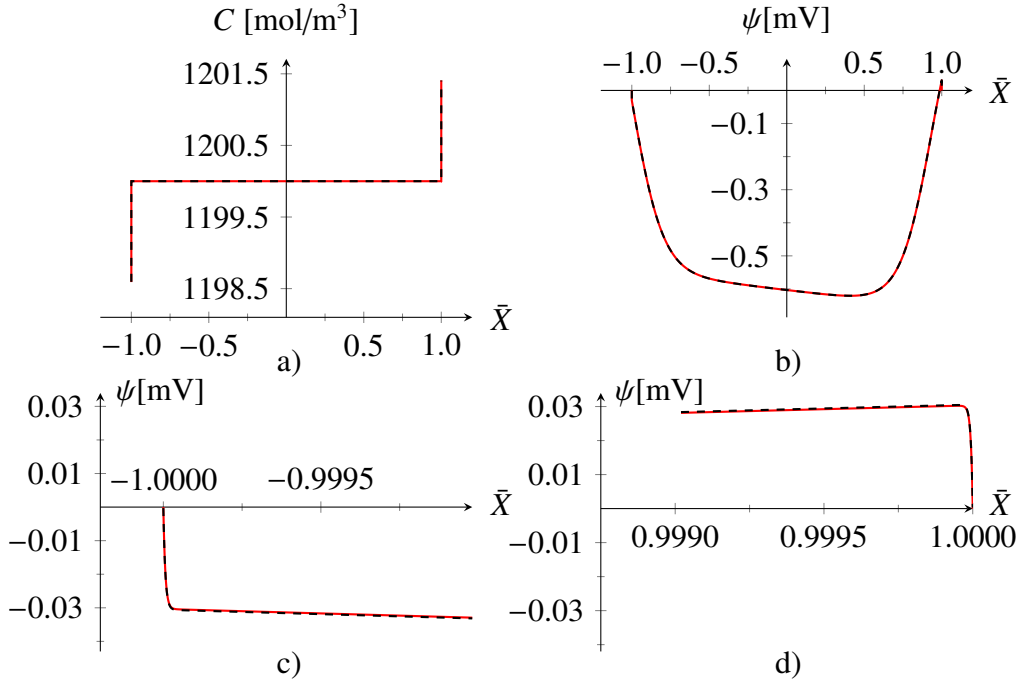

Figure 4. Particularisation of the present model (black line) to compression sensing without CLs [23] (red line): comparison in terms of counterions concentration and electric potential.

Figure 4b shows the results in terms of electric potential, confirming the excellent match, as definitely demonstrated by the details in the boundary layer regions displayed in Figure 4c,d. Note that in the model without CLs [23] we directly apply a null electric potential at $X = \pm h$ through the short-circuit condition. This is in a very good agreement with the present particularisation of the new solution, which predicts very small values of electric potential, $\psi(\pm h, t_f) = \pm 3.0265 \times 10^{-7}$ mV, at the ionomer-CL interfaces. Moreover, the counterions flux is totally negligible in the CLs, where the electric potential linearly goes to zero at $X = \pm(h + d)$, i.e., where we apply the short-circuit condition. We finally note that the asymmetric behaviour of $\psi(X, t)$ with respect to $X = 0$, due to the chosen asymmetry in the elastic modulus, is particularly relevant at $X = \pm h$. At these points ψ must have opposite signs in order to maintain the same gradient, this last feature being required by the short-circuit and ion-blocking conditions in view of the linearisation of the electric current (2.4).

4.2. Finite element analyses: implementation of linear equations

The accuracy of the analytical solution presented in Section 3 is further verified through FE analyses performed with the commercial software COMSOL Multiphysics®. To this aim, we implement the uncoupled linearised PDEs (2.1) and (2.5) in three different FE domains.

By using the COMSOL Mathematics interface, Eqs (2.11) and the two systems (2.14) are separately solved in the nondimensional spatial domains $[-1, 1]$, $[-1 - d/h, -1]$, and $[1, 1 + d/h]$, respectively. We

remark that in the FE analyses we always adopt only X as spatial variable to describe the geometry. The ionomer-CL interface conditions on electric potential, ion flux, electric displacement, and counterions concentration (see Eqs (2.7) and (2.8)) are imposed through Dirichlet and Flux/Source conditions at the interfaces between the domains. Dirichlet conditions at $\bar{X} = -1 - d/h$ and $\bar{X} = 1 + d/h$ are also introduced to enforce the short-circuit and ion-blocking conditions (2.9).

The analyses are performed by discretising each domain with 8000 elements distributed in symmetric arithmetic sequence, by selecting element ratio equal to 1000. This specific mesh, characterised by extremely small elements at the boundaries of each domain, permits an accurate evaluation of the solution in the boundary layer regions, where it may be subject to large gradients. The equations are solved by the parallel sparse direct linear solver MUMPS, whereas the backward differentiation formulas are employed for time integration.

Differently from the example of Section 4.1, here the CLs are characterised by: $\epsilon_{\pm}^* = 1$, $\mathcal{D}_{\pm}^* = 1$, $\phi_{\pm} = 0.5$, and $d/h = 0.01$. Moreover, for what concerns the boundary layers, we set $\nu = 0.6$ and $\delta = 10^{-5}$. However, we still use the deformation of Figure 3, reached at the time $t_f = 0.5$ ms, to trigger the sensing response.
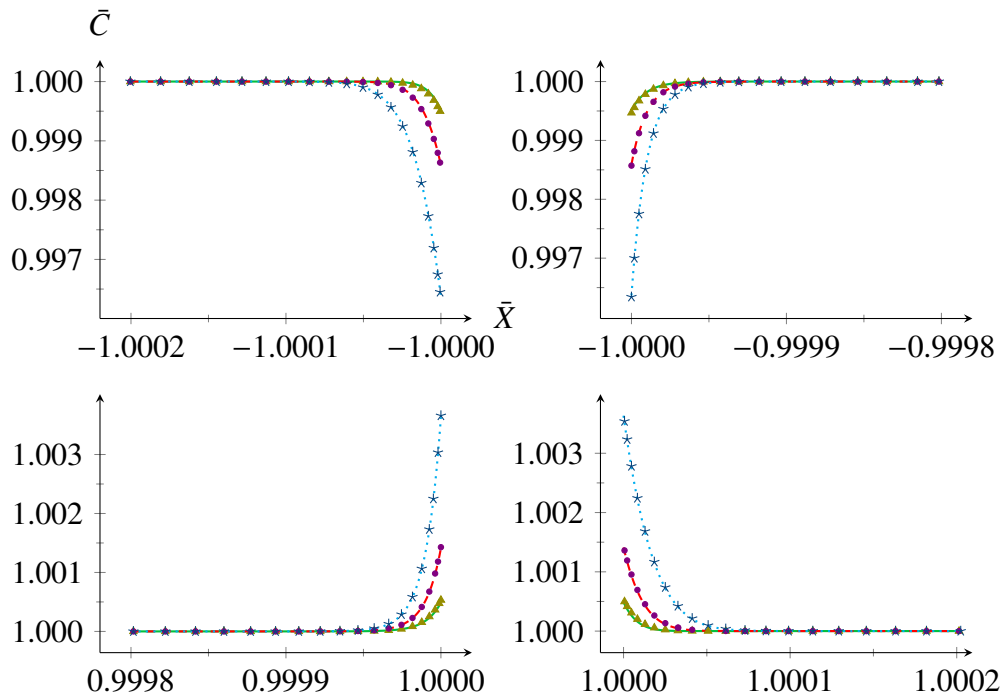

Figure 5. Comparison between analytical (lines) and FE (symbols) results for the linearised modified PNP system: nondimensional counterions concentration at the ionomer-CL interfaces, evaluated at the different instants $t_f/\Delta t$ (blue dotted line versus stars), $t_f/(2\Delta t)$ (red dashed line versus circles), and $t_f/(4\Delta t)$ (green solid line versus triangles), with $\Delta t = 0.1$ ms and $t_f = 0.5$ ms.

Figures 5 and 6 show an excellent match between analytical and numerical results, by displaying concentration and electric potential in the ionomer and in the CLs near the interfaces, at three different instants of the analysis. In these regions, the model predicts the formation of boundary layers of

counterions concentration (see Figure 5), whose magnitude increases with time. At the end of the analysis, the boundary layers occupy the regions $\bar{X} \in [\approx -1.00005, \approx -0.99995]$ and $\bar{X} \in [\approx 0.99995, \approx 1.00005]$, whose size is on the order of δ. We highlight that the boundary layer size is approximately constant in the ionomer, while it varies in the CLs, where ions slowly diffuse. This is the reason why the CL-electrode interfaces are free from boundary layers.

The qualitative profile of the electric potential is totally analogous to that in the absence of CLs (as displayed in the particularisation of Figure 4b for $\bar{X} \in [-1, 1]$), except that here ψ assumes relatively small but non-vanishing values at the ionomer-CL interfaces, and then linearly decreases to zero at the electrodes. This is shown in the first and fourth graphs of Figure 6, which focuses on the ionomer-CL regions, whose main feature is the formation of boundary layers (i.e., large gradient of ψ) in the ionomer (see second and third graphs of Figure 6). We remark that these boundary layers, whose magnitude largely increases with time, provide an immediate measure of the short-circuit electric current generated through the IPMC in this sensing benchmark.
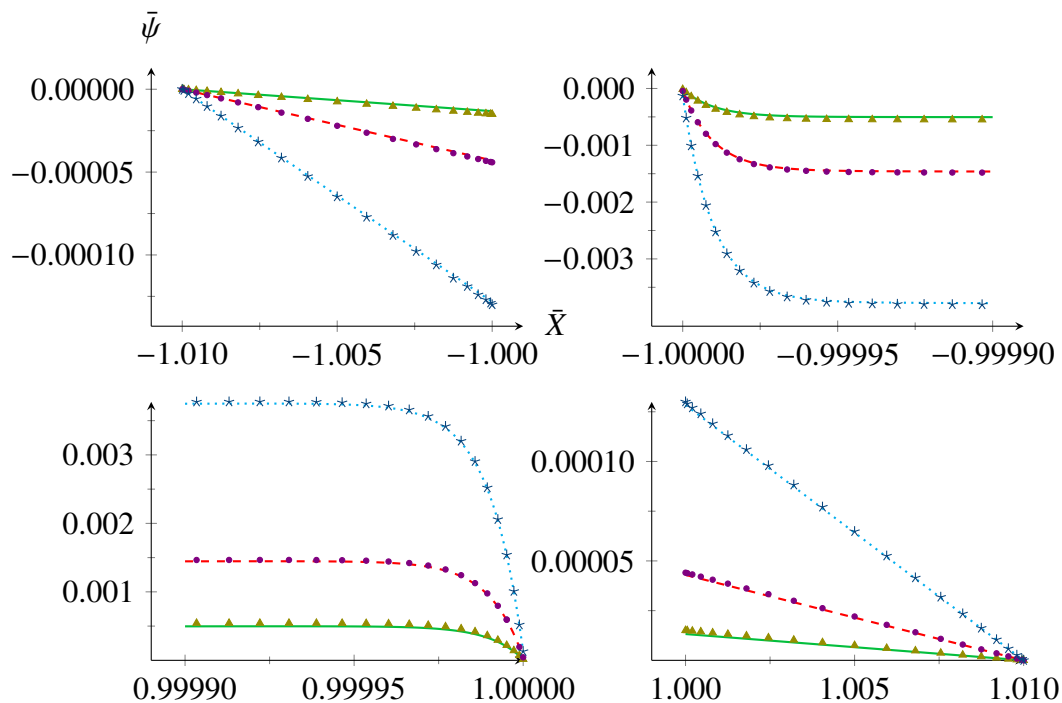

Figure 6. Comparison between analytical (lines) and FE (symbols) results for the linearised modified PNP system: nondimensional electric potential at the ionomer-CL interfaces, evaluated at the different instants $t_f/\Delta t$ (blue dotted line versus stars), $t_f/(2\Delta t)$ (red dashed line versus circles), and $t_f/(4\Delta t)$ (green solid line versus triangles), with $\Delta t = 0.1$ ms and $t_f = 0.5$ ms.

5. Discussion of the analytical solution against numerical analysis of the fully coupled nonlinear problem

Here we finally critically assess the analytical solution developed in Section 3. To this purpose, we compare its results with those of numerical analyses solving the fully coupled nonlinear problem

governing IPMC compression sensing, where the linear momentum balance must be solved together with the modified PNP system, in which the displacement $u(X, t)$ is a further unknown field.

In the ionomer region, the following system of governing PDEs holds:

$$\frac{\partial S(X, t)}{\partial X} = 0 \tag{5.1a}$$

$$\frac{\partial D(X, t)}{\partial X} = \mathcal{F}[C(X, t) - C_0] \tag{5.1b}$$

$$\frac{\partial J(X, t)}{\partial X} + \frac{\partial C(X, t)}{\partial t} = 0 \tag{5.1c}$$

Equation (5.1a) is the linear momentum balance in the absence of body forces, where S is the through-the-thickness direct component of the *nominal* stress, given by the sum of three contributions [4, 23]: the mechanical stress due to membrane stretching, S_{mec}, the osmotic stress related to counterions mixing, S_{osm}, and the polarisation stress related to dielectric polarisation, S_{pol}. Eqs (5.1b) and (5.1c) are the Gauss law and the mass balance, respectively, written with respect to the reference configuration.

Similarly, in the CL regions the governing equations read

$$\frac{\partial S_{\pm}^{\text{cl}}(X, t)}{\partial X} = 0 \tag{5.2a}$$

$$\frac{\partial D_{\pm}^{\text{cl}}(X, t)}{\partial X} = \mathcal{F}[C_{\pm}^{\text{cl}}(X, t) - C_0\,\phi_{\pm}] \tag{5.2b}$$

$$\frac{\partial J_{\pm}^{\text{cl}}(X, t)}{\partial X} + \frac{\partial C_{\pm}^{\text{cl}}(X, t)}{\partial t} = 0 \tag{5.2c}$$

where $S_{\pm}^{\text{cl}}$ indicates the relevant stress component in the CLs.

We conveniently solve the problem in nondimensional form, by employing the following expressions for the nominal stress, electric displacement, and counterions flux [23]:

$$\bar{S} = \underbrace{\alpha\left(1 + \frac{\partial \bar{u}}{\partial \bar{X}}\right)\left[\frac{\partial \bar{u}}{\partial \bar{X}} + \frac{1}{2}\left(\frac{\partial \bar{u}}{\partial \bar{X}}\right)^2\right]}_{\text{mechanical stress}} + \underbrace{\delta^2 \frac{1}{2\left(1 + \frac{\partial \bar{u}}{\partial \bar{X}}\right)^2}\left(\frac{\partial \bar{\psi}}{\partial \bar{X}}\right)^2}_{\text{polarisation stress}}$$

$$+ \underbrace{\frac{-1 + 2\nu}{(-1 + \nu)\nu}\left[-\ln\left(1 - \frac{2\nu}{1 + \frac{\partial \bar{u}}{\partial \bar{X}}}\right) + \ln\left(1 - \frac{\nu(1 + \bar{C})}{1 + \frac{\partial \bar{u}}{\partial \bar{X}}}\right)\right]}_{\text{osmotic stress}} \tag{5.3a}$$

$$\bar{D} = -\delta^2 \frac{1}{1 + \frac{\partial \bar{u}}{\partial \bar{X}}} \frac{\partial \bar{\psi}}{\partial \bar{X}} \tag{5.3b}$$

$$\bar{J} = -\delta\left[\frac{(-1 + 2\nu)(-1 + \nu - \frac{\partial \bar{u}}{\partial \bar{X}})}{(\nu - 1)\left(\nu\bar{C} - 1 + \nu - \frac{\partial \bar{u}}{\partial \bar{X}}\right)\left(1 + \frac{\partial \bar{u}}{\partial \bar{X}}\right)^2} \frac{\partial \bar{C}}{\partial \bar{X}} - \bar{C}\frac{\partial \bar{\psi}}{\partial \bar{X}}\frac{1}{\left(1 + \frac{\partial \bar{u}}{\partial \bar{X}}\right)^2}\right.$$

$$
- \frac{-1 + 2\nu}{(\nu - 1)\left(\nu\bar{C} - 1 + \nu - \frac{\partial \bar{u}}{\partial \bar{X}}\right)\left(1 + \frac{\partial \bar{u}}{\partial \bar{X}}\right)^2} \bar{C} \frac{\partial^2 \bar{u}}{\partial \bar{X}^2} \Bigg] \quad (5.3c)
$$

where the nondimensional variables are defined by employing the scaling parameters introduced in Section 2.2, along with $C_0 \mathcal{RT}$, both for the stress and to define the nondimensional elastic modulus

$$
\alpha = \frac{\lambda(X) + 2\mu(X)}{C_0 \mathcal{RT}}
$$

with λ and μ denoting the Lamé constants, which are in general spatially variable in the membrane. Here, within the Cha and Porfiri [4] theory, the mechanical stress (work conjugate to the deformation gradient) is governed by the Saint-Venant–Kirchhoff strain energy density (which is quadratic in the Green-Lagrange strain tensor through λ and μ); the polarisation stress and the electric displacement are determined by the conventional free energy density contribution quadratic in the Eulerian electric field through the permittivity; the osmotic stress is given by a free energy density term statistically accounting for ion mixing that modifies the proposal of Borukhov et al. [32]. Such term also contributes to the electrochemical potential, in turn giving a constraint to the dissipative constitutive prescription for the counterions flux. For further details the reader is referred to [4, 23].

Analogously, in the CLs:

$$
\bar{S}_{\pm}^{\text{cl}} = \alpha_{\pm}^{\text{cl}}\left(1 + \frac{\partial \bar{u}_{\pm}^{\text{cl}}}{\partial \bar{X}}\right)\left[\frac{\partial \bar{u}_{\pm}^{\text{cl}}}{\partial \bar{X}} + \frac{1}{2}\left(\frac{\partial \bar{u}_{\pm}^{\text{cl}}}{\partial \bar{X}}\right)^2\right] + \phi_{\pm}\ \epsilon_{\pm}^* \delta \frac{1}{2\left(1 + \frac{\partial \bar{u}_{\pm}^{\text{cl}}}{\partial \bar{X}}\right)^2}\left(\frac{\partial \bar{\psi}_{\pm}^{\text{cl}}}{\partial \bar{X}}\right)^2
$$

$$
+ \phi_{\pm} \frac{-1 + 2\nu}{(-1 + \nu)\nu}\left[-\ln\left(1 - \frac{2\nu}{1 + \frac{\partial \bar{u}_{\pm}^{\text{cl}}}{\partial \bar{X}}}\right) + \ln\left(1 - \frac{\nu(1 + \bar{C}_{\pm}^{\text{cl}})}{1 + \frac{\partial \bar{u}_{\pm}^{\text{cl}}}{\partial \bar{X}}}\right)\right] \quad (5.4a)
$$

$$
\bar{D}_{\pm}^{\text{cl}} = -\phi_{\pm}\ \epsilon_{\pm}^* \delta \frac{1}{1 + \frac{\partial \bar{u}_{\pm}^{\text{cl}}}{\partial \bar{X}}} \frac{\partial \bar{\psi}_{\pm}^{\text{cl}}}{\partial \bar{X}} \quad (5.4b)
$$

$$
\bar{J}_{\pm}^{\text{cl}} = -\phi_{\pm}\ \mathcal{D}_{\pm}^* \delta^2 \Bigg[\frac{(-1 + 2\nu)(-1 + \nu - \frac{\partial \bar{u}_{\pm}^{\text{cl}}}{\partial \bar{X}})}{(\nu - 1)\left(\nu\bar{C}_{\pm}^{\text{cl}} - 1 + \nu - \frac{\partial \bar{u}_{\pm}^{\text{cl}}}{\partial \bar{X}}\right)\left(1 + \frac{\partial \bar{u}_{\pm}^{\text{cl}}}{\partial \bar{X}}\right)^2} \frac{\partial \bar{C}_{\pm}^{\text{cl}}}{\partial \bar{X}}
$$

$$
+ \bar{C}_{\pm}^{\text{cl}} \frac{\partial \bar{\psi}_{\pm}^{\text{cl}}}{\partial \bar{X}} \frac{1}{\left(1 + \frac{\partial \bar{u}_{\pm}^{\text{cl}}}{\partial \bar{X}}\right)^2} + \frac{-1 + 2\nu}{(\nu - 1)\left(\nu\bar{C}_{\pm}^{\text{cl}} - 1 + \nu - \frac{\partial \bar{u}_{\pm}^{\text{cl}}}{\partial \bar{X}}\right)\left(1 + \frac{\partial \bar{u}_{\pm}^{\text{cl}}}{\partial \bar{X}}\right)^2} \bar{C}_{\pm}^{\text{cl}} \frac{\partial^2 \bar{u}_{\pm}^{\text{cl}}}{\partial \bar{X}^2}\Bigg] \quad (5.4c)
$$

where $\alpha_{\pm}^{\text{cl}} = (\lambda_{\pm}^{\text{cl}} + 2\mu_{\pm}^{\text{cl}})/(C_0 \mathcal{RT})$ with $\lambda_{\pm}^{\text{cl}}$ and $\mu_{\pm}^{\text{cl}}$ denoting the Lamé constants in the CLs.

We remark that the linearisation of expressions (5.3) and (5.4), along with neglecting the electrochemical stresses in the balances (5.1a) and (5.2a), leads to the linear modified PNP systems (2.1) and (2.5) modulated by the *a priori* computed displacement field.

We complete the problem formulation by adding the interface, boundary, and initial conditions. For the electrochemistry, we apply conditions (2.18), (2.19) and (2.20), whereas, for what concerns the mechanics, we impose the continuity of displacement and stress at the ionomer-CL interfaces

$$
\bar{u}(\pm 1, \bar{t}) = \bar{u}_{\pm}^{\text{cl}}(\pm 1, \bar{t}) \quad (5.5a)
$$

$$\bar{S}(\pm 1, \bar{t}) = \bar{S}^{\mathrm{cl}}_{\pm}(\pm 1, \bar{t}) \tag{5.5b}$$

along with the boundary conditions represented in Figure 1

$$\bar{u}^{\mathrm{cl}}_{-}(-1 - d/h, \bar{t}) = 0 \tag{5.6a}$$

$$\bar{u}^{\mathrm{cl}}_{+}(1 + d/h, \bar{t}) = \hat{u}(\bar{t}) \tag{5.6b}$$

and the initial conditions

$$\bar{u}(\bar{X}, 0) = 0 \tag{5.7a}$$

$$\bar{u}^{\mathrm{cl}}_{\pm}(\bar{X}, 0) = 0 \tag{5.7b}$$

We implement the systems (5.1) and (5.2) by using the COMSOL Mathematics interface. We use a finer mesh than that employed for the validation in Section 4.2, as we discretise the three spatial domains $[-1, 1]$, $[-1 - d/h, -1]$, and $[1, 1 + d/h]$ with 10000 elements each. To capture the large gradients characterising the interface regions, we choose element ratio equal to 1000.

We set the CL thickness such that $d/h = 0.01$ and select the other parameters as follows. About the electrochemistry: $C_0 = 1200$ mol/m^3, $\nu = 0.25$, $\delta = 10^{-5}$, $\phi_{\pm} = 0.5$, $\epsilon^*_{\pm} = 1$, and $\mathcal{D}^*_{\pm} = 1$. About the mechanics, we adopt $\alpha(X)$ as in [23], in order to provide the deformation of Figure 3 in the purely mechanical compression problem, and α^{cl}_{+} and α^{cl}_{-} are spatially variable parameters obtained by simply extending the function $\alpha(X)$ in the CLs. We remark that the (large) magnitude of α^{cl}_{+} and α^{cl}_{-} has a very limited impact on the IPMC sensing response because the boundary layers of ψ occur in the ionomer at the ionomer-CL interfaces.

The comparison between analytical and numerical results is reported in Figure 7 in terms of the time evolution of the observed electric current per unit surface area. For both models, we employ the linearised definition of $i(t)$, which is proportional to the difference in the electric potential gradient at the boundary layers. However, note that the definition of $i(t)$ accounting for nonlinearities provides similar results. We evaluate the electric response for the three different applied displacements $\hat{u}(t_{\mathrm{f}}) = 1$ μm, $\hat{u}(t_{\mathrm{f}}) = 2.5$ μm, and $\hat{u}(t_{\mathrm{f}}) = 5$ μm, linearly increasing within the same time $t_{\mathrm{f}} = 0.5$ ms.

For relatively small applied displacement, we observe a good match between analytical and FE solutions. However, as the applied displacement increases, the analytical solution turns out to underestimate the electric response evaluated with the fully coupled nonlinear FE model. This behaviour agrees with the results in the absence of CLs, for which the effect of nonlinearities has been thoroughly analysed in [23]. We remark that, even in the case with the largest difference ($\hat{u}(t_{\mathrm{f}}) = 5$ μm), the deformation field in the membrane predicted by the FE model is basically coincident with that obtained by solving the linear momentum balance in terms of mechanical stress only (by the way, such deformation is displayed in Figure 3); therefore, the source of the discrepancy in Figure 7 should not be sought in the uncoupling the analytical solution relies on, while it is due to the nonlinear interaction between electrochemical and mechanical fields in the counterions flux. Moreover, we observe that the discrepancy between analytical and FE results obtained in the presence of CLs is slightly larger than that highlighted in [23]. This may be ascribed to the complex behaviour of the electrochemical fields in the ionomer-CL interface regions. In fact, in the presence of CLs, the boundary layers in the ionomer, with respect to those at the ionomer-electrode interfaces in the absence of CLs, are smoother due to the possibility of counterions to diffuse in the CLs. This

behaviour may challenge the asymptotic technique, whose capability to provide a faithful solution depends on the actual relevance of the boundary layers.
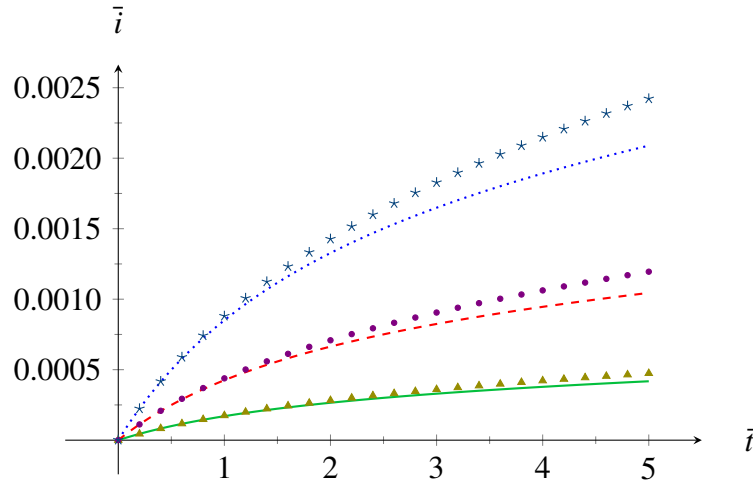

Figure 7. Comparison between analytical (lines) and FE (symbols) results for the fully coupled nonlinear system of governing PDEs: nondimensional electric current per unit surface area in time, evaluated for different values of the applied displacement: $\hat{u}(t_f) = 1$ μm (green solid line vs triangles), $\hat{u}(t_f) = 2.5$ μm (red dashed line vs circles), and $\hat{u}(t_f) = 5$ μm (blue dotted line vs stars).

6. Parametric analysis

To provide an insight on both the electrochemomechanical behaviour and the relevance of the analytical solution towards IPMC design, here we study the influence of some key parameters on IPMC compression sensing. The accurate determination of such parameters, which highly depend on the manufacturing process and the chosen materials, both concurring in establishing the IPMC specific microstructure, turns out to be a very difficult task. Recent efforts on IPMC additive manufacturing [12, 33, 34] should reduce uncertainties in the IPMC microstructure, hopefully making our study useful for IPMC characterisation through inverse analysis.

We investigate a relatively wide range of meaningful values for the parameters ν, $\phi_\pm$, and d/h, whereas we set $\epsilon_\pm^* = 1$, $\mathcal{D}_\pm^* = 1$, $\delta = 10^{-5}$, $C_0 = 1200$ mol/m^3, and $h = 100$ μm. Moreover, in all the analyses we apply the deformation field of Figure 3, which leads to a nondimensional mechanical stress $\bar{S}_{\text{mec}} = -0.150259$. These data ensue from the variation of the elastic properties set in [23] along the membrane, having, far enough from the interfaces, Young modulus equal to 497 MPa and Poisson ratio equal to 0.49.

First, we explore the influence of the counterions packing capability by varying the steric coefficient, $0.1 \leq \nu \leq 0.999$, and by setting $\phi_\pm = 0.5$ and $d/h = 0.01$. We report the results in Figure 8, in terms of electric potential in the boundary layer regions, and in Table 1, in terms of electric current and maximum values of osmotic and polarisation stresses.
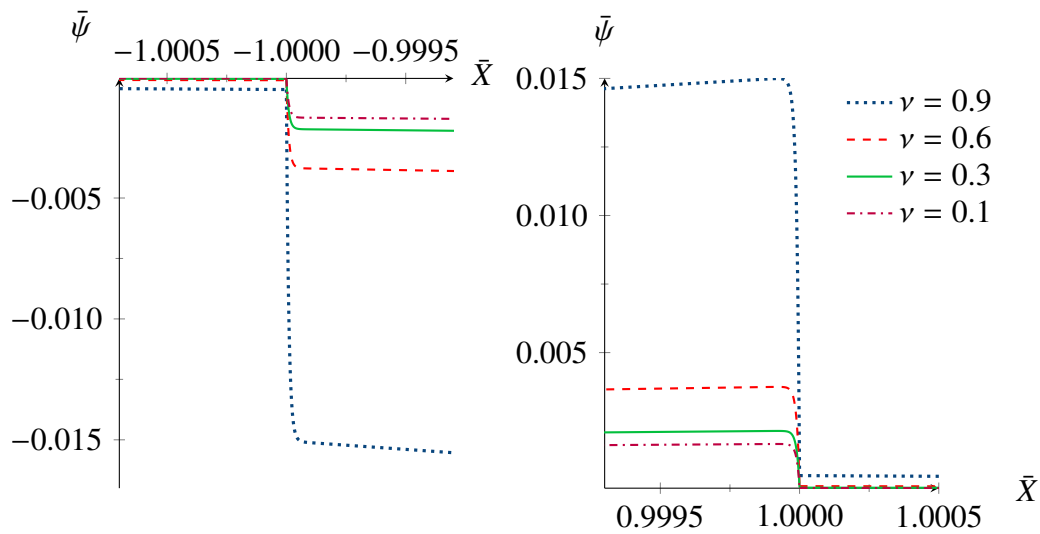
Figure 8. Effect of the steric coefficient, ν: electric potential in the two ionomer-CL interface regions for applied displacement $\hat{u}(t_{\mathrm{f}}) = 5\ \mu$m.

Table 1. Effect of the steric coefficient, ν: nondimensional electric current per unit surface area and maximum values of the nondimensional electrochemical stresses.

ν	i	S_{osm}	S_{pol}
0.1	0.00174106	3.66375×10^{-6}	2.66431×10^{-9}
0.3	0.0022385	6.16008×10^{-6}	4.40427×10^{-9}
0.6	0.00391738	-1.73499×10^{-5}	1.34881×10^{-8}
0.9	0.0156695	2.89178×10^{-4}	2.15809×10^{-7}
0.999	1.56695	-1.79024	0.00215809

The electric current is clearly magnified as the steric coefficient increases, leading to larger electrochemical stresses. In fact, *for a given deformation*, augmenting the difficulty encountered by counterions in packing at the interfaces increases the observed electric response. We note that within the analytical solution ν has to be suitably lower than 1 in order to avoid too large electrochemical stresses, that would be inconsistent with the uncoupling of the linear momentum balance this solution is based on. Hence, most likely, the results of Table 1 for the case $\nu = 0.999$ (undisplayed in Figure 8) are largely inaccurate. We note, however, that the FE analysis of the fully coupled nonlinear problem experiences lack of convergence even for ν larger than about 0.5, by adopting the discretisation illustrated in Section 5. A reliable solution for ν close to 1 seems to be a very difficult task and would require a much more complex and expensive numerical model. Instead, in the cases $\nu = \{0.1, 0.3, 0.6, 0.9\}$, the maximum values of osmotic and polarisation stresses, here always reached in the ionomer at the ionomer-CL interfaces, are several order of magnitude lower than the mechanical stress, according to the results in the absence of CLs [23]. The electrochemical stresses increase with the steric coefficient, resulting about two order of magnitude larger by changing ν from 0.1 to 0.9.

Second, we analyse the influence of the ionomer volume fraction in the CLs, $0.3 \leq \phi_\pm \leq 0.7$, by setting $v = 0.25$ and $d/h = 0.01$. As transparent from Figure 9, an increase of $\phi_\pm$ leads to a decrease of the electric potential jump in the ionomer at the interfaces, this being proportional to the electric current. In fact, the presence of a large number of metal particles in the CLs (low $\phi_\pm$) should hamper the counterions diffusion in the CLs (see Eq (5.4c) for the flux in the CLs), thus resulting in larger boundary layers in the ionomer. For the sake of completeness, the resulting electrochemical stresses are reported in Table 2.
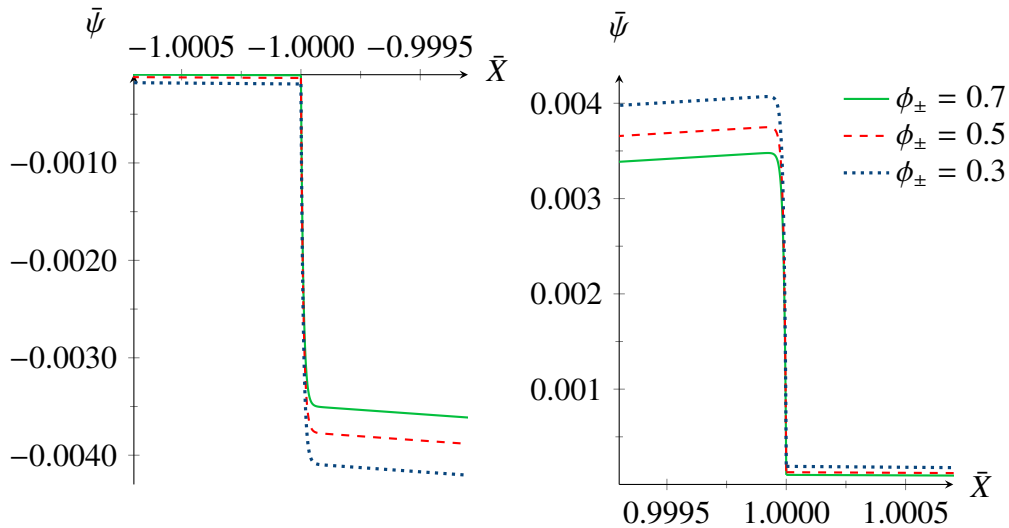

Figure 9. Effect of the ionomer volume fraction in the CLs, $\phi_\pm$: electric potential in the two ionomer-CL interface regions for applied displacement $\hat{u}(t_f) = 5\ \mu m$.

Table 2. Effect of the ionomer volume fraction in the CLs, $\phi_\pm$: nondimensional electric current per unit surface area and maximum values of the nondimensional electrochemical stresses.

$\phi_\pm$	i	S_{osm}	S_{pol}
0.3	0.00291039	5.71139×10^{-6}	4.40607×10^{-9}
0.5	0.00208927	5.3298×10^{-6}	3.83661×10^{-9}
0.7	0.00169863	4.97396×10^{-6}	3.34111×10^{-9}

Finally, we investigate the effect of the CL thickness, $0.01 \leq d/h \leq 0.04$, by setting $v = 0.25$ and $\phi_\pm = 0.5$. The results listed in Table 3 show that the electric response slightly reduces as the CL thickness increases. This is because the counterions diffusion in the CLs diminishes with the CL thickness, thus leading to larger counterions accumulation at the ionomer-CL interfaces, according to the foregoing remarks.

Table 3. Effect of the CLs thickness, d/h: nondimensional electric current per unit surface area and maximum values of the nondimensional electrochemical stresses.

d/h	i	S_{osm}	$S_{\max}$
0.01	0.00208927	5.3298×10^{-6}	3.83661×10^{-9}
0.02	0.00203463	5.22375×10^{-6}	3.68535×10^{-9}
0.03	0.00198230	5.12129×10^{-6}	3.54209×10^{-9}
0.04	0.00193216	5.02224×10^{-6}	3.40632×10^{-9}

7. Concluding remarks

In this work, we have presented in detail the analytical solution for the short-circuit electric response of Ionic Polymer Metal Composites (IPMCs) subjected to a through-the-thickness displacement. This benchmark, referred to as compression sensing, has been studied in [23] for the case of spatially uniform electrochemical properties along the entire membrane, i.e., the IPMC ionomer where mobile ions diffuse. Here, as a main novelty, we have accounted for the presence of Composite Layers (CLs), which are very thin interphase regions between ionomer and electrodes, resulting from manufacturing, where the presence of metal particles leads to large variations of the electrochemical properties with respect to the plain membrane [15–17].

In particular, we have analytically solved the problem governed by three *modified* Poisson-Nernst-Planck (PNP) systems, describing the IPMC electrochemistry in the ionomer and in each CL. Here, the term *modified* refers to the role of the displacement field in modulating the PNP system, to be solved for the mobile ions concentration and the electric potential [4]. Moreover, a suitably small applied displacement in IPMC sensing allows one to *a priori* obtain the displacement field from the linear momentum balance by neglecting the electrochemical stresses, and to linearise the modified PNP systems [10]. Given that the IPMC electrochemistry is governed by boundary layers of mobile ions concentration and electric potential, we have approached the problem by resorting to the perturbative method of matched asymptotic expansions.

We have validated and discussed the obtained analytical solution by comparison with the results of Finite Element (FE) analyses. In particular, we have assessed its limits of validity against the FE solution of the fully nonlinear problem, coupling, in each region, the modified PNP system with the linear momentum balance. Moreover, we have employed the analytical solution both to establish an equivalent circuit model, clarifying how IPMC compression sensing works, and to perform parametric analyses, elucidating the effect of some relevant parameters on the sensing response.

Towards the design of optimised IPMC sensors, future efforts should first focus on the IPMC characterisation, with the purpose of unveiling the complex relation between the electrochemomechanics of IPMCs and their microstructure. We expect that the present analytical solution can play a role in this important process, by resorting to inverse analysis and an *ad hoc* experimental campaign which should leverage on the possibility of tailoring the geometrical and material properties of IPMCs. Among the many aspects involved in such a challenging process, let us mention that IPMC additive manufacturing [12, 33, 34] may permit, for instance, a design in which an ionomeric layer close to one of the electrodes has suitably different modulus with respect to the rest of the membrane. First of all, this would allow one to have unprecedented control on the IPMC

compression sensing by *a priori* establishing the main source of the mechanical asymmetry, thus making the direction of the counterions flux known. Second, the results of tests on different IPMCs manufactured with differently thick ionomeric layers of variable modulus should help in identifying the model parameters through inverse analysis.

Acknowledgements

Conflict of interest

The authors declare that they have no conflict of interest.

References

1. Shahinpoor M, Kim KJ (2001) Ionic polymer-metal composites: I. Fundamentals. *Smart Mater Struct* 10: 819–833.

2. Oguro K, Takenaka H, Kawam Y (1993) Actuator element. *US Patent* 5268082.

3. Kim KJ, Shahinpoor M (2003) Ionic polymer-metal composites: II. Manufacturing techniques. *Smart Mater Struct* 12: 65–79.

4. Cha Y, Porfiri M (2014) Mechanics and electrochemistry of ionic polymer metal composites. *J Mech Phys Solids* 71: 156–178.

5. Wallmersperger T, Akle BJ, Leo DJ, et al. (2008) Electrochemical response in ionic polymer transducers: An experimental and theoretical study. *Compos Sci Technol* 68: 1173–1180.

6. Porfiri M (2008) Charge dynamics in ionic polymer metal composites. *J Appl Phys* 104: 104915.

7. Nemat-Nasser S, Li JY (2000) Electromechanical response of ionic polymer-metal composites. *J Appl Phys* 87: 3321–3331.

8. Aureli M, Porfiri M (2013) Nonlinear sensing of ionic polymer metal composites. *Continuum Mech Therm* 25: 273–310.

9. Leronni A, Bardella L (2019) Influence of shear on sensing of ionic polymer metal composites. *Eur J Mech A-Solid* 77: 103750.

10. Porfiri M (2019) Sensing mechanical deformation via ionic polymer metal composites: A primer. *IEEE Instru Meas Mag* 22: 8868271.

11. Nemat-Nasser S (2002) Micromechanics of actuation of ionic polymer-metal composites. *J Appl Phys* 92: 2899–2915.

12. Carrico JD, Tyler T, Leang KK (2017) A comprehensive review of select smart polymeric and gel actuators for soft mechatronics and robotics applications: fundamentals, freeform fabrication, and motion control. *Int J Smart Nano Mater* 8: 144–213.

13. Porfiri M, Leronni A, Bardella L (2017) An alternative explanation of back-relaxation in ionic polymer metal composites. *Extreme Mech Lett* 13: 78–83.

14. Boldini A, Porfiri M (2020) Multiaxial deformations of ionic polymer metal composites. *Int J Eng Sci* 149: 103227.

15. Tiwari R, Kim KJ (2010) Effect of metal diffusion on mechanoelectric property of ionic polymer-metal composite. *Appl Phys Lett* 97: 244104.

16. Cha Y, Aureli M, Porfiri M (2012) A physics-based model of the electrical impedance of ionic polymer metal composites. *J Appl Phys* 111: 124901.

17. Cha Y, Porfiri M (2013) Bias-dependent model of the electrical impedance of ionic polymer metal composites. *Phys Rev E* 87: 022403.

18. Borukhov I, Andelman D, Orland H (1997) Steric effects in electrolytes: A modified poisson-boltzmann equation. *Phys Rev Lett* 79: 435–438.

19. Kilic MS, Bazant MZ, Ajdari A (2007) Steric effects in the dynamics of electrolytes at large applied voltages. I. Double-layer charging. *Phys Rev E* 75: 021502.

20. Kilic MS, Bazant MZ, Ajdari A (2007) Steric effects in the dynamics of electrolytes at large applied voltages. II. Modified Poisson-Nernst-Planck equations. *Phys Rev E* 75: 021503.

21. Porfiri M (2009) Influence of electrode surface roughness and steric effects on the nonlinear electromechanical behavior of ionic polymer metal composites. *Phys Rev E* 79: 041503.

22. Aureli M, Porfiri M (2012) Effect of electrode surface roughness on the electrical impedance of ionic polymer-metal composites. *Smart Mater Struct* 21: 105030.

23. Volpini V, Bardella L, Rodella A, et al. (2017) Modelling compression sensing in ionic polymer metal composites. *Smart Mater Struct* 2: 035030.

24. Kocer BY (2014) *Experimental study of ionic polymer metal transducers: characterization of transient response in sensing*, PhD thesis of Swanson School of Engineering, University of Pittsburgh.

25. Porfiri M, Sharghi H, Zhang P (2018) Modeling back-relaxation in ionic polymer metal composites: The role of steric effects and composite layers. *J Appl Phys* 123: 014901.

26. Verhulst F (2005) *Methods and Applications of Singular Perturbations*, Springer.

27. Cheng DK, (1983) *Field and Wave Electromagnetics*, Addison-Wesley Publishing Company.

28. Wallmersperger T, Akle BJ, Leo DJ, et al. (2004) Coupled chemo-electro-mechanical formulation for ionic polymer gels–numerical and experimental investigations. *Mech Mater* 36: 411–420.

29. Crank J, (1975) *The Mathematics of Diffusion*, Oxford University Press.

30. Wolfram S (2011) *Wolfram Mathematica — Release 8.0.1.0*, Champaign, IL, USA.

31. Bard AJ, Faulkner LR (2001) *Electrochemical Methods. Fundamentals and Applications*, John Wiley & Sons.

32. Borukhov I, Andelman D, Orland H (2000) Adsorption of large ions from an electrolyte solution: A modified Poisson-Boltzmann equation. *Electrochim Acta* 46: 221–229.

33. Carrico JD, Traeden NW, Aureli M, et al. (2015) Fused filament 3D printing of ionic polymer-metal composites (IPMCs). *Smart Mater Struct* 24: 125021.

34. Stalbaum T, Trabia S, Hwang T, et al. (2018) Guidelines for making ionic polymer-metal composite (IPMC) materials as artificial muscles by advanced manufacturing methods, In: Bar-Cohen, Y., *Advances in Manufacturing and Processing of Materials and Structures*, CRC Press, 379–395.